1980

A mechanistic study of the hydrogenolysis of neopentane on iridium

Nancy Ellen Kinkade
Iowa State University

KINKADE, NANCY ELLEN

A MECHANISTIC STUDY OF THE HYDROGENOLYSIS OF NEOPENTANE ON IRIDIUM

Iowa State University PH.D. 1980

A mechanistic study of the hydrogenolysis of neopentane on iridium

by

Nancy Ellen Kinkade

A Dissertation Submitted to the
Graduate Faculty in Partial Fulfillment of the
Requirements for the Degree of
DOCTOR OF PHILOSOPHY

Department: Chemistry
Major: Physical Chemistry

Approved:

Signature was redacted for privacy.

In Charge of Major Work

Signature was redacted for privacy.

For the Major Department

Signature was redacted for privacy.

For the Graduate College

Iowa State University
Ames, Iowa

1980

TABLE OF CONTENTS

	Page
INTRODUCTION	1
LITERATURE REVIEW	3
EXPERIMENTAL	14
High Vacuum System Design	14
Thin Film Deposition	19
Kinetic Data Collection Procedure	20
LEED, Auger and Flash Desorption Procedures	27
Materials	30
RESULTS AND DISCUSSION	32
Surface Characterization	32
Thin Film Characterization	38
Difficulties Encountered in Conducting Kinetic Experiments	44
Results of Kinetic and Deuterium Exchange Experiments	55
Mechanistic Considerations	60
SUMMARY AND SUGGESTIONS FOR FUTURE INVESTIGATIONS	97
LITERATURE CITED	99
ACKNOWLEDGMENT	103

INTRODUCTION

It is not surprising that hydrogenolysis reactions have been extensively studied because of their importance in coal liquefaction, petroleum reforming and other processes. In order to develop an ideal catalyst for one of these processes it is important to understand the mechanism involved and thus the hydrogenolysis of many hydrocarbons has been studied. Most of the studies have involved ethane or propane on various supported and unsupported catalysts while far fewer have involved higher hydrocarbons. This study was undertaken to determine the mechanism of the hydrogenolysis of neopentane (2,2-dimethylpropane) on iridium films.

Neopentane is an interesting molecule to study because it is the smallest hydrocarbon which contains a quaternary carbon atom and hence is unable to undergo α-β diadsorption, the proposed mode of adsorption of ethane in the hydrocracking of ethane over iron (1) and nickel (2).

Iridium was chosen as the catalyst because it exhibits high activity for hydrogenolysis reactions, yet it has not been examined to a large extent. This will probably change in the future because iridium-platinum alloys have been found to be excellent reforming catalysts (3,4). Although few kinetic studies have been completed on iridium, there do exist several adsorption studies which will help characterize surface species important in the hydrogenolysis reaction.

This thesis will describe the kinetic and isotopic studies leading to a proposed reaction mechanism as well as the LEED, Auger and flash desorption studies which yield further evidence in support of the mechanism. The work will be discussed in three sections starting with a review of the pertinent literature, followed by the description of the experimental methods and finally presentation of results and discussion.

LITERATURE REVIEW

There are very few kinetic studies on the hydrogenolysis of neopentane, however, there are several studies concerned with product distributions and with the relative activities of catalysts for isomerization and hydrogenolysis. First, the general results of these studies will be discussed and then the mechanistic implications.

Two different reactions are possible when neopentane and hydrogen are reacted. First, neopentane can be isomerized to isopentane and/or n-pentane and second, carbon-carbon bonds can be broken and hydrogen added to the fragments to form lower hydrocarbons. All of the group VIII metals plus copper and gold have been found to be active for the hydrogenolysis reaction, while only platinum (5-9), gold (5), tungsten (8), palladium (10), and iridium (5,11) catalyze the isomerization reaction. Anderson and Avery (7) found that iridium films were not active for isomerization but Boudart and Ptak (5) later reported that the supported iridium catalyst they studied did isomerize neopentane and attributed their findings to a greater sensitivity of their analytical apparatus. New light has been shed on this question by Foger and Anderson (11), who found that iridium supported on either γ-alumina or silica will isomerize neopentane if the mean particle size is large (7 and 20 nm), but not if the mean particle size is small (<2 nm). Thus it

is possible that the catalyst employed by Boudart and Ptak (5) contained some particles of large mean particle size while the films used by Anderson and Avery (7) were well dispersed. A similar trend was observed for platinum (12). The authors found that the tendency for neopentane isomerization decreased with decreasing mean platinum particle size below about 20 nm, and most of this change occurred for particles below about 1.5 nm in size. This trend follows approximately the variation in the proportion of surface atoms in (111) facets and thus agrees with the hypothesis (6) that the isomerization reaction is surface sensitive.

There have been three studies on the reaction of deuterium and neopentane (13-15) in which films of nickel, iron, cobalt, tungsten, palladium and rhodium were used as the catalysts. These studies discuss both the exchange and hydrogenolysis reactions on the first three metals, but only exchange for the latter three. The ratio of the rate of exchange to the rate of hydrogenolysis was 6.5, 2, and 1 over nickel, iron and cobalt respectively. Over iron films the only initial products were $(CH_3)_3(CH_2D)C$ and $(CH_3)_3(CD_3)C$. Over nickel, cobalt and palladium films the major products were the same as for iron films; however, nickel and palladium yielded predominantly the mono-deuterated species and cobalt the multiply deuterated species. Over both nickel and cobalt films some of the initially exchanged neopentanes contained more than three deuteriums and thus indicate an

α,γ exchange process. Tungsten and rhodium were also reported to yield multiply exchanged products.

The deuterolysis of neopentane over iron films resulted in the production of 99% perdeuteromethane and small quantities of perdeuteroisobutane. Because of the absence of exchange at more than one carbon atom of neopentane on iron films, the authors concluded that the α,γ diadsorbed intermediate was strongly and irreversibly adsorbed and led directly to carbon-carbon bond rupture. Over nickel and cobalt films methane was still the major product although nickel yielded more of the intermediate hydrocarbons (isobutane, propane and ethane) than did cobalt. Once again all of the deuterolysis products were completely exchanged.

The studies on the hydrogenolysis of neopentane will be discussed in two sections depending on whether the catalyst involved was supported or unsupported. The product distributions obtained over metal films and palladium black are shown in Table I. As can be seen, the distributions vary depending on the catalyst employed. Nickel and iron films crack neopentane extensively yielding mainly methane while the other metals produce less methane and more of the higher hydrocarbons. It is interesting to note that the more n-butane (an isomerization product) produced, the less methane is produced. Thus platinum, the best isomerization catalyst of the group, yields the smallest amount of methane.

Table I. Product distributions obtained from the reaction of neopentane over a variety of metal films.

Catalyst	T(K)	Distribution of Products (%)[a] M	E	P	iso-B	n-B	Ref.
Ni	503	95	4	1			9
	503	97	3				8
W	475	57	17	11	15		9
	475	41	17	14	18	10	8
	492	60	15	15	4	6	8
Rh	430	73	18	4	5		8,9
Pt	569	25	14	17	27	17	9
	569	17	9	12	38	24	8
Pd-black	558	57.2	1.7	3.36	34.6	3.33	10
	585	58.2	1.12	2.81	33.5	4.63	10
Fe[b]	486	99			1		13
	516	99.8			0.2		13

[a]M=methane; E=ethane; P-propane; iso-B=iso-butane; n-B=n-butane.

[b]Products from the reaction of neopentane and deuterium.

Table II. Activation energies for the hydrogenolysis of neopentane over various metal films.

Catalyst	T(K)	$E(\frac{kcal}{mole})$	$\log(\frac{A}{mole/cm^2/sec.})$	Ref.
Nickel	496-538	32	26.3	8
Tungsten	475-492	11	17.5	8
Iron[a]	446-486	38	--	13
Pd-black	558	53.5	31.46	10
Platinum	512-563	21	21.2	16

[a]Deuterolysis of neopentane.

Table II shows the activation energies and frequency factors for the hydrogenolysis of neopentane on films of nickel, tungsten, iron and palladium black.

The reactant pressures used in the studies by Anderson and Baker(8,9) and Dowie et al. (13) were ~3 torr neopentane and 40 → 45 torr hydrogen. Sárkány et al. (10) used 10 torr neopentane and 23.7 → 750 torr hydrogen in their study over a palladium black catalyst. They reported reaction orders with respect to hydrogen of 0.67 → -1.5 at 558K and 1.1 → -1.35 at 585K although they did not report any orders with respect to neopentane.

The work on the supported catalysts resulted in more kinetic studies yielding orders of the reaction with respect to the reactants in addition to product distributions and activation energies. The product distributions vary depending on the particular catalyst as occurred for the unsupported catalysts. The activation energies vary from 30 to 60 kcal/mole depending on the catalyst used (5). For iridium the activation energies reported are 46 kcal/mole for 10% Ir/SiO_2 (5) and 55 to 60 kcal/mole for iridium of various dispersions supported on SiO_2 and γ-Al_2O_3 (11).

The orders of the reaction (n,m) with respect to both reactants as indicated by equation (1)

$$\text{rate} \propto P_{C_5H_{12}}^{n} \; P_{H_2}^{m} \qquad (1)$$

are summarized in Table III and can be seen to differ

Table III. Kinetic pressure dependence exponents for the hydrogenolysis of neopentane over various catalysts.

Catalyst	Pressure Range (torr)	n	m	Ref.
Ir(γ-Al_2O_3, SiO_2)	P_{H_2}, 20-101 $P_{C_5H_{12}}$, 1.3-12	1	-2.9	11
Ru(γ-Al_2O_3)	b	0.89	-0.87	17
Pt(Aerosil)	P_{H_2}, 450-750 $P_{C_5H_{12}}$, 9.7-90	0.7	-0.9	12
	P_{H_2}, 150-370 $P_{C_5H_{12}}$, 13-45	0.04	+0.3	
Pt((La)y-zeolite)	P_{H_2}, 200-750 $P_{C_5H_{12}}$, 13-68	1	-1.5	12
Rh(γ-Al_2O_3)	P_{H_2}, 50-200 $P_{C_5H_{12}}$, 5-20	1	-1.5	18
Pt+Mo(SiO_2)	P_{H_2}, 25-750 $P_{C_5H_{12}}$, 25-100	1	+1 → 0	19
Pt(SiO_2)	P_{H_2}, 25-750 $P_{C_5H_{12}}$, 25-100	1	+1 → 0.3	19

[a] $\text{Rate} \propto P_{C_5H_{12}}^{n} P_{H_2}^{m}$.

[b] Total pressure = 800 torr (pressure ranges not given).

substantially from study to study. The hydrogen orders vary from +1 to -2.9 and the neopentane orders from 1 to 0.4. Only when the pressure range was very large did any one study show that the hydrogen or neopentane order varied and was not constant as indicated by the studies which utilized smaller pressure ranges.

Now that the general results of the studies involving neopentane have been summarized, the proposed intermediates and mechanisms for the reaction of hydrogen and neopentane will be discussed. Anderson and Avery (7) proposed that the intermediates involved in the hydrogenolysis and isomerization of neopentane are identical because they found the same activation energy for the two reactions. The activation energies for the hydrogenolysis of neopentane were found to differ substantially from those for ethane. This is to be expected if a diadsorbed intermediate is involved, because neopentane is unable to α-β diadsorb, while that is the only mode available to ethane. Adsorption at a single metal atom was not proposed because it would be difficult to explain the observed surface sensitive nature of the isomerization reaction. Thus Anderson and Avery (7) proposed the intermediates shown in Figure 1. The triadsorbed intermediate was invoked to explain the enhancement of the selectivity for isomerization of neopentane on evaporated films of platinum exposing the (111) faces predominantly. This

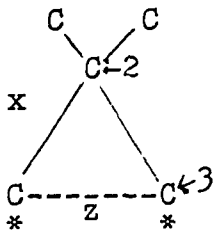

α,γ diadsorbed
(a)

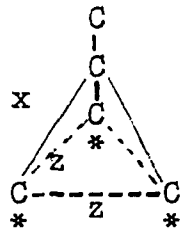

triadsorbed
(b)

Figure 1. The proposed intermediates for neopentane hydrogenolysis and isomerization (7).

enhancement was also observed for isobutane but not for n-butane and thus the triadsorbed intermediate was proposed because it can be formed by both isobutane and neopentane but not by n-butane. With the diadsorbed intermediate shown in Figure 1(a), a cyclic intermediate may be formed when a bond labeled z is formed. When the bond at x ruptures, isomerization will occur if the bond at z is formed, while hydrogenolysis will result if no bond at z is formed. The situation is different in the case of the triadsorbed intermediate for here there are two equivalent positions at which bond z may be formed when bond x ruptures. Thus for isomerization to occur only one of the two possible bonds must be formed while in the case of hydrogenolysis, neither of the two z bonds can form when the bond at x breaks. Anderson and Baker (9) explain that the reduced rate of deuterium exchange of neopentane on nickel at higher temperatures is probably due to the formation of strongly adsorbed species which are multiply bonded to the surface. On this basis

Figure 1(a) might be more realistically represented as shown below.

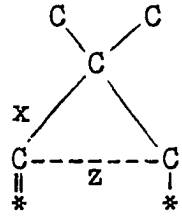

α, α, γ triadsorbed intermediate

To explain their results, Foger and Anderson (12) proposed that two different parallel pathways exist which have different activation energies and whose relative proportions are particle size dependent. Pathway 1 involves one or both of the multiply bonded analogs of the intermediates shown in Figure 1. Pathway 2 must occur at a platinum site which is relatively abundant for a mean particle size of 1 nm, but whose relative abundance falls rapidly as the particle size increases and must also be capable of yielding high selectivity toward hydrogenolysis. The authors felt that a model in which pathway 2 operates at a single surface atom would accommodate their results best. Further they propose that a low coordination atom (corner or edge atom) would be a favored reaction site since the surface concentration of such atoms increases rapidly in the range of mean particle size less than about 2 nm. In order to accept pathway 2, there must be a mechanism for the skeletal rearrangement of

hydrocarbons at a single atom site. Two such mechanisms have previously been proposed (20-23) and Foger and Anderson have adapted one of them as shown below.

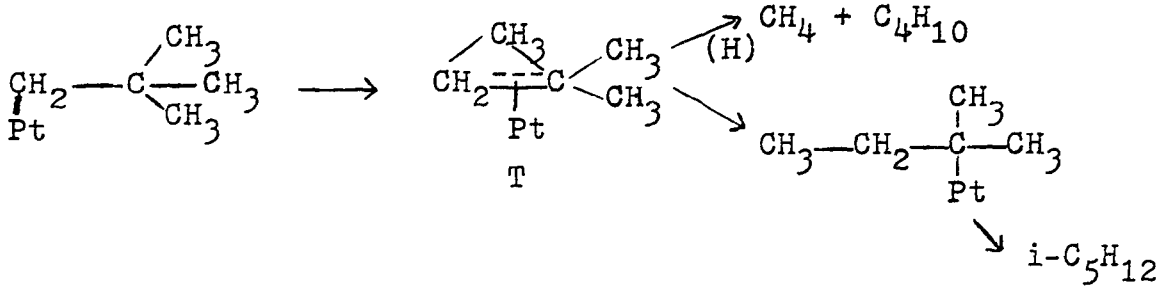

Thus the choice between isomerization and hydrogenolysis would be dependent on the ratio of concentrations of adsorbed hydrogen and hydrocarbon. Rooney (24) does not feel that it is very likely that the transition state species T shown above will be involved in the hydrogenolysis reaction as proposed by Foger and Anderson (12) because of energetic considerations. He proposed the following two alternative reactions as possible mechanisms for hydrogenolysis at a single metal atom (M).

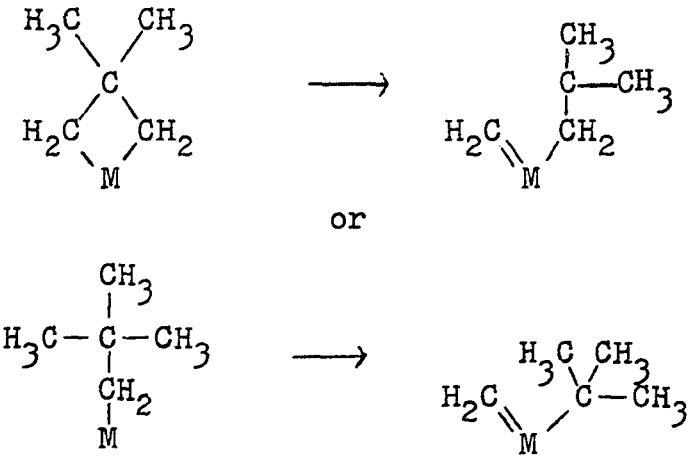

It is obvious from the above review that there is no universally accepted mechanism, which is due in part to the absence of good kinetic studies covering a wide pressure range which would allow the elucidation of a rate expression.

EXPERIMENTAL

The hydrogenolysis of neopentane was investigated *via* several different types of experiments. Most of the work involved the collection of kinetic data using a high vacuum system and thin films. Auger electron spectroscopy was used to identify surface species while low energy electron diffraction was used to characterize the surface symmetry. Flash desorption experiments were carried out to identify species adsorbed on the surface. A single crystal was used in the Auger, LEED and flash desorption experiments. All of the methods involved will be thoroughly discussed in the following sections.

High Vacuum System Design

A pyrex glass and 304 stainless steel system pumped by rotary pumps, mercury diffusion pumps and an ion pump were used to collect the kinetic data. A schematic of the system is shown in Figure 2. The system is functionally divided into two sections; a manifold in which the reactant gases are mixed, and the high vacuum portion containing the catalyst and the mass spectrometer. Pressure measurements were made in various ways depending on the pressure to be measured. At pressures $>10^{-4}$ torr a thermocouple gauge was used; pressures in the range 10^{-4} to 10^{-10} torr were

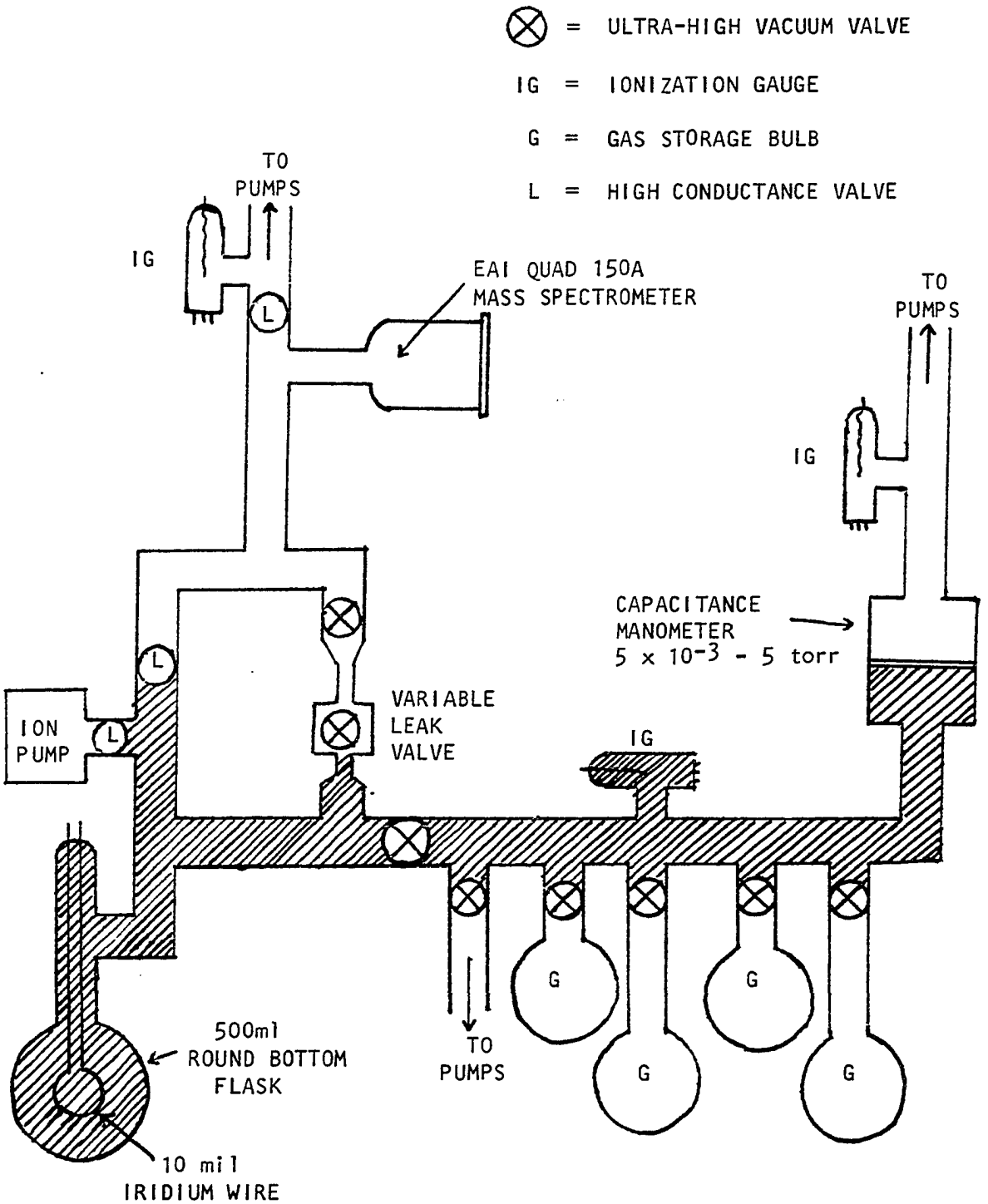

Figure 2. Schematic of the high vacuum system used for kinetic studies. (Shaded area = reaction volume = 1500 cc.)

measured using a conventional Bayard-Alpert ionization gauge; pressures of gases dosed into the manifold were measured with a capacitance manometer (Granville-Phillips, Series 212, Boulder, Colorado). The manometer on this system could measure pressures in the range 10^{-4} to 5 torr after being calibrated against a McLeod gauge (Consolidated Vacuum Corporation, Type GM 100A, Rochester, New York) using argon. Pressure (torr) was related to scale deflection using a power curve of the form:

$$\text{Pressure (torr)} = A \cdot (\text{scale deflection})^{B}$$

where $0.9 < B < 1.1$ or a linear equation of the form:

$$\text{Pressure (torr)} = C + D \cdot (\text{scale deflection})$$

The calibration was checked several times and was found to remain constant within 10%. To prevent zero drift the manometer head was thermostatted at 301.4K by circulating water from a constant temperature bath through a water jacket. The reactant gases were premixed in the manifold before being expanded into the reaction cell. The best vacuum attainable in the manifold was 10^{-8} torr with a double stage Hg diffusion pump and a 1-N_2 trap. The reference side of the capacitance manometer was kept at $\sim 10^{-7}$ torr with a single stage Hg diffusion pump and a 1-N_2 trap.

The high vacuum portion of the system could be pumped to a pressure of 10^{-10} torr using a 20 l/sec. differential ion pump (Ultek, Model #60-063) after a pressure of 10^{-9}

torr had been attained *via* triple and double stage Hg diffusion pumps and a $l\text{-}N_2$ trap connected in series. Of course both the manifold and high vacuum side were initially pumped to 10^{-3} torr using rotary pumps with $l\text{-}N_2$ traps prior to turning on the diffusion pumps.

The high vacuum side includes a 500 ml round bottom glass flask reaction cell in which an 8 cm length of 10 mil iridium wire was spotwelded to two nickel feedthroughs. A film could then be deposited on the walls of the flask as described in the next section. The reaction cell could be heated to any temperature between room temperature and 775K by raising a tube furnace (S. B. Lindberg, type SP, Watertown, Wisconsin) around it. The temperature was then monitored by either a chromel-alumel or iron-constantan thermocouple which was inside the furnace and in direct thermal contact with the glass bulb. Once thermal equilibrium was attained the temperature remained constant to within $\pm 2°C$.

The reaction mixture was leaked from the reaction volume (the high vacuum and manifold portions of the system) through a variable leak valve (Granville-Phillips Company, series 203, Boulder, Colorado) to the differentially pumped mass spectrometer (AEI Quad 150A). The conductance of the leak valve was continuously variable from 100 cc per second to 10^{-10} cc per second. The leak valve was set so that the mass spectrometer, which could operate in the range 10^{-11} to

10^{-5} torr, was at a pressure of 10^{-7} to 10^{-5} torr during the course of the experiment and so that less than 10% of the reactants would be leaked out of the reaction volume, which was thus essentially a static reactor, during any run. The mass spectrometer was connected to a dual channel strip chart recorder (Clevite Corporation, Brush Recorder Mark 280, Cleveland, Ohio). During kinetic runs mass peaks at 1 to 30 a.m.u. were monitored every 5 sec. for the duration of the run (2 to 5 min.). At various times masses up to 80 a.m.u. were monitored to determine if any hydrocarbons besides methane were being produced. Rapid scans during leak tests, etc. were displayed on an oscilloscope (Tektronix, Inc., Type R.M. 503).

The volumes of the manifold and high vacuum portion of the system were needed in order to determine the pressure of the reactants in the reaction cell. This was easily obtained by using argon and a standard volume attached to the manifold *via* an ultra-high vacuum valve. The volume of the manifold and reaction cell were found to be 490 and 1007 cm^3 respectively and thus the reaction volume (shaded section in Figure 2) was 1497 cm^3.

The system could be heated to 623K with a portable oven and heating tapes to help reduce the background pressure of water, carbon monoxide and carbon dioxide so that a minimum pressure of 10^{-10} torr could be attained.

Thin Film Deposition

Only the procedures used in the study will be discussed because several excellent reviews on thin film techniques already exist (25,26). A 500 ml round bottom flask was cleaned with soap and water followed by acetone prior to being glassblown onto the high vacuum system. The system was then heated, as mentioned in the previous section, in order to obtain a pressure in the 10^{-10}torr range. The 8 cm piece of 10 mil iridium wire spotwelded to the nickel feedthroughs was resistively heated in order to outgas it. The wire was heated for a day or two until it was possible to heat it hot enough to evaporate the iridium without having the background pressure rise above 3×10^{-8} torr. When a film was being deposited the current was cycled on and off in 5 sec. intervals so that the nickel feedthroughs would not heat up very much, thereby reducing their outgassing. Table IV shows the procedure used to deposit film #8 on which much of the kinetic data was collected. Before the film was used, it was sintered at a temperature ~10°C above the maximum temperature which would be encountered during the kinetic experiments. This was done because it has been reported that unsintered iridium films have unstable catalytic activity (27). Films were also deposited with the reaction cell initially at the sintering temperature. Both

Table IV. Procedure for deposition of iridium film #8 from an 8 cm length of iridium wire by resistive heating.

Time (min.)	Current[a] (amps)	Background Pressure (torr)	Temperature (K)
0	4.8	4×10^{-8}	300
12	5.0	4×10^{-8}	300
30	5.1	4×10^{-8}	300
51	5.2	4×10^{-8}	300
59	5.3	4×10^{-8}	300
66	5.4	4×10^{-8}	300
74	5.6	4×10^{-8}	300
94	5.7	4×10^{-8}	300
134	OFF	2×10^{-8}	started heating
154		5×10^{-8}	482
164[b]		5×10^{-8}	furnace off

[a] 5 sec. on/off cycle.

[b] Dosed 1 torr hydrogen into the hot cell.

methods resulted in deposition of a very thin, uniform film active for the neopentane hydrogenolysis and stable from day to day.

Kinetic Data Collection Procedure

Kinetic data were collected at temperatures in the

range 403-473K with most of the data taken at 468K. The pressure ranges studied were 10^{-3} to 0.25 torr and 10^{-2} to 3 torr for neopentane and hydrogen respectively. To collect data from which the order of the reaction with respect to one of the reactants was to be obtained, the pressure of the other reactant was held constant while the pressure of the reactant of interest was varied. In all cases the reactants were first dosed into the manifold using the capacitance manometer to measure pressures and then expanded into the reaction cell. An expansion curve, such as the one shown in Figure 3, was used to calculate the pressure after expansion. If no adsorption of the reactants occurred then a constant expansion factor could be used, however this is not the case for either neopentane or hydrogen and thus curves such as the one shown in Figure 3 are obtained. The neopentane case will be discussed in further detail in a later section.

The reaction was monitored by partial pressure analysis of the reaction mixture from the mass spectra of the gas mixture in the reaction cell leaked through the variable leak valve. The mass spectrometer consisted of three sections: ionizing region, quadrupole mass filter and electron multiplier. In the first section gas molecules were ionized by 80 volt electrons emitted by a tungsten-3% rhenium filament heated by a variable current of 0.25 to 3.0 mA (usually

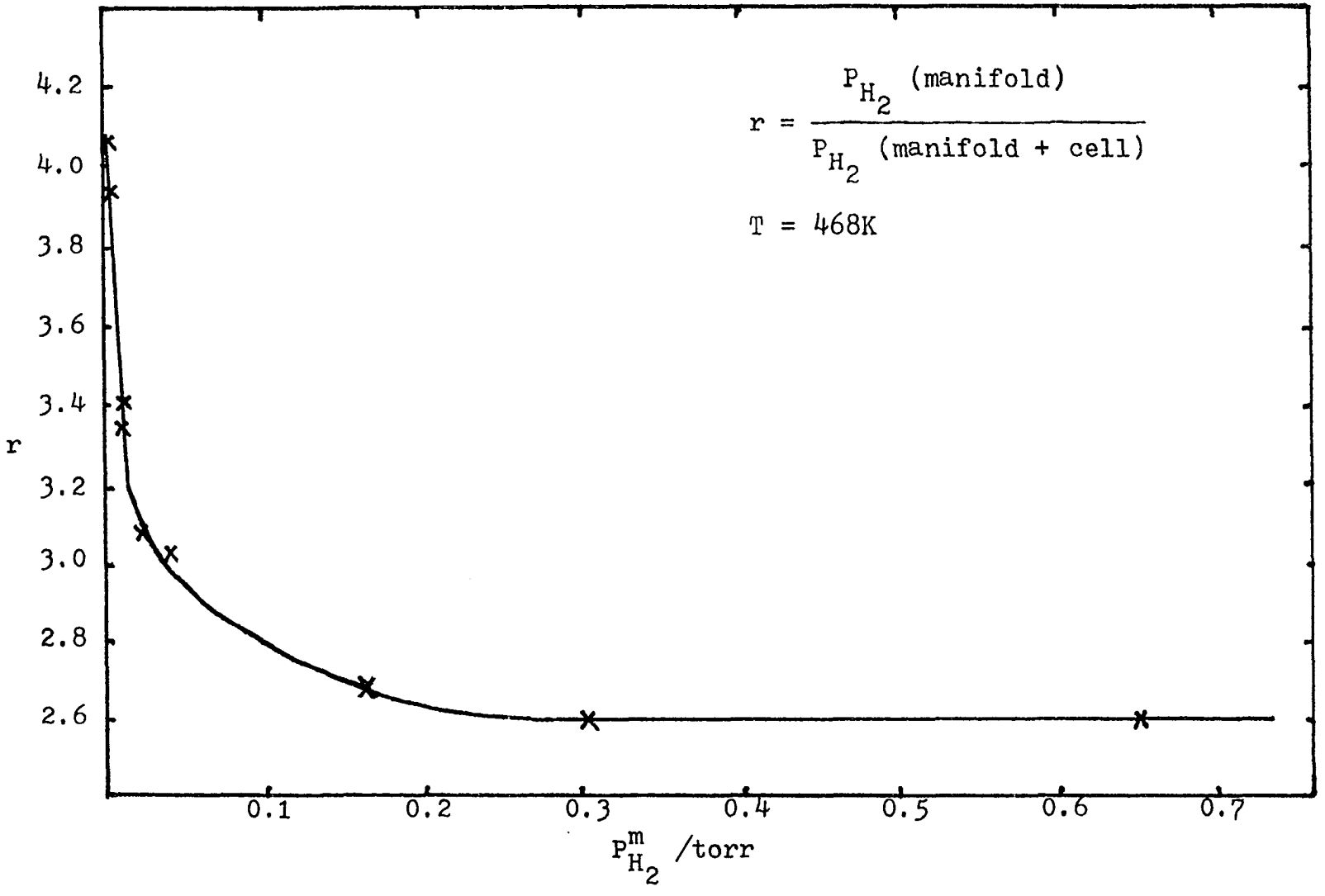

Figure 3. The variation of the hydrogen expansion factor as a function of the pressure of hydrogen in the manifold.

set at 0.8 mA). The ions were then accelerated and focused by electrostatic lenses into the quadrupole filter where only ions with certain mass per charge (m/z) ratios were allowed to traverse the entire length of the rods. A DC voltage with superimposed RF voltage was applied to opposite pairs of rods -- one pair being at negative potential and the other positive. The voltages were applied in a sawtooth sweep and the ions passed through the filter in order of increasing m/z ratio as the voltage was swept from low to high potentials. Ions which successfully passed through the filter rod assembly impinged upon the first dynode of the electron multiplier while the other ions were neutralized by striking some internal surface and then were pumped out of the system as a gas. The electron multiplier was a 14-stage beryllium-copper detector consisting of 13 dynodes (electrodes) and an anode. The current resulting from positive ions impinging on the first dynode was amplified through the fourteen stages with gains achieved typically above 10^5 when a 3000 volt potential drop across the multiplier was used. At fixed emission current the ion current i_m for a species of mass m was proportional to the pressure of the parent species

$$i_m = q_m \cdot P$$

where the sensitivity q_m is a constant. The ion current used here is the electron multiplier output, although,

strictly speaking, it should be the unamplified current at the first dynode of the multiplier; hence q_m depended directly on the multiplier gain. The sensitivity was determined over the entire pressure range (to be used during a subsequent set of experiments) to determine if it decreased at high pressures indicating saturation of the electron multiplier. Saturation of the multiplier was overcome by decreasing 1) the electron multiplier gain by using a Fluke high voltage power supply (John Fluke Manufacturing Company, Incorporated, Mountlake Terrace, Washington, model 410B) to reduce the potential drop across the multiplier, 2) the electron emission of the filament thereby reducing the number of ions produced, or 3) the pressure at the mass spectrometer by adjusting the variable leak valve.

Another problem which had to be checked for periodically involved the flow of gases through the variable leak. It is necessary that the gas mixture passing through the mass spectrometer correctly reflects the composition in the reaction cell. If the flow is molecular, lighter gases will have a higher conductance through the leak than will the heavier gases since molecular flow exhibits an inverse dependence on the square root of the molecular weight of the gas. Opening the orifice wider would alleviate this problem so that the flow depended only on the partial pressures of the gases and not on their molecular weights.

In all of the experiments the only product obtained was methane and thus the reaction was monitored by observing the change in the height of the mass spectral peak at m/z=16. This peak was monitored instead of m/z=15 because neopentane exhibits a large peak corresponding to 15 a.m.u. There is overlap at m/z=16 with background water; however, the amount of background water is small (compared to the amount of methane produced) and constant, so that this was not a problem. In order to convert the amount of methane observed in the mass spectral output (millivolts) to a pressure (torr) a plot of sensitivity (10^{-3} torr/mv) versus pressure was constructed. The sensitivity remained constant when only methane was dosed into the cell; however, if the pressure of another gas was varied the sensitivity would also vary. These results will be discussed in detail in a later section.

Between each run the reactant cell was flushed with hydrogen at the reaction temperature so that any reactive carbon remaining on the surface after evacuating the neopentane and hydrogen could be removed. If this was not done, some methane would be produced in a subsequent kinetic run which was not due solely to the neopentane introduced during that particular run. The hydrogen was left in the cell until no increase in the methane peak was observed and the amount of methane produced during the flush was used to calculate the surface area of the catalyst active for the

adsorption of neopentane.

When there were no experiments being conducted the film was stored at room temperature in 1 torr of hydrogen. The amount of methane in the cell at the end of a set of runs could be compared with the amount present after the film had been exposed to hydrogen overnight to determine if carbon had been left on the surface which was not readily removed by a hydrogen flush.

The kinetic data were taken to obtain the order of the reaction with respect to neopentane, hydrogen and methane. Also runs in which the pressures of neopentane and hydrogen were held constant and the temperature was varied were conducted in order to determine the activation energy for the reaction. All the rates are expressed as turnover numbers (molecules of methane-site^{-1}-sec.$^{-1}$) which allows comparison with other data in the literature since the turnover numbers are not explicitly dependent upon the catalyst surface area. In order to calculate the turnover numbers, the number of sites had to be determined which was accomplished by using the methane desorption data obtained during a hydrogen flush. The amount of methane desorbed increased when the neopentane pressure during the run prior to the flush was increased until a plateau was reached. The value of the maximum amount of methane desorbed was used in the ideal gas law to determine the number of molecules desorbed which can be taken

as the number of sites available for neopentane adsorption. The surface area of the catalyst can be calculated if it is assumed that there is, for instance, one iridium atom per site and that there are 10^{15} sites/cm^2 (calculated value for a close packed surface). The first assumption is questionable at best and consequently only the number of surface sites is calculated and no assumption on the number of atoms per site is made. All of the rates reported are initial rates. The reaction was monitored for approximately 2 minutes with the mass spectrometer scanning 0-30 a.m.u. every 5 seconds. As mentioned previously, the production of hydrocarbons other than methane was checked for periodically.

In some cases deuterium was used in place of hydrogen as will be discussed later.

LEED, Auger and Flash Desorption Procedures

LEED, Auger and flash desorption experiments were conducted so that a greater understanding of the reactions occurring on the surface might be possible. LEED and Auger are two surface sensitive techniques, the first being used to determine the surface structure of a crystal and relate the structure of an adsorbed ordered overlayer to that surface structure, and the second to determine an elemental analysis of the adsorbates and the first few monolayers of the surface. Excellent reviews of LEED (28,29) and Auger

(30,31) are available.

The LEED/Auger experiments were performed in a Varian 981-2000 vacuum system with 4 grid LEED optics and an Auger cylindrical mirror analyzer. The base pressure of 2×10^{-10} torr was attainable by baking the system to 250°C and by using both ion pumps and titanium sublimation pumps. The sample was mounted in an offset manipulator with x, y and z translation and 360° rotary motion. The sample could be conductively heated *via* an indirect heater block to 1500K. The temperature was measured by a tungsten/5% rhenium, tungsten/26% rhenium thermocouple spotwelded to the face of the sample. The sample could be cleaned by argon ion bombardment by an ion gun located in the bell jar which was connected to a glass manifold system pumped by a rotary pump and Hg diffusion pumps *via* a Granville-Phillips variable leak valve so that gases could be dosed into the Varian system. Pressure measurements were made with an ion gauge, mercury manometer or thermocouple gauges. The bell jar was also equipped with a mass spectrometer (Uthe Technology International, Model 100C Precision Gas Analyzer, Sunnyvale, California) for analysis of gas species.

The Auger spectra were run with 10μA filament emission current and a beam energy of 2000 eV. At this low beam current little heating of the sample or disruption of the overlayer occurred. The peak-to-peak modulation voltage was

5 volts, the scan rate used was either 200 eV/min. or 66.6 eV/min. and the spectra (5-550 eV) were recorded on an x-y recorder. The LEED patterns were taken using a beam voltage of 160-180 eV and an emission current ~2.2amps.

The flash desorption experiments were also conducted in this system. Neopentane was dosed on the sample until the desired dosage was obtained, the surface was analyzed with LEED and Auger and then rotated in front of the mass spectrometer and flashed. The sample could be heated to 1100°C in 60 sec. with temperature increase proportional to flash time. The mass spectra were recorded using a Brush strip chart recorder and the change in temperature, as measured by the thermocouples, was recorded by a Moseley x-y recorder. In this way any desorption peaks could be related to the temperature at which they occurred. The mass spectrometer scanned 0-65 a.m.u. each second so that production of hydrocarbons with a maximum of 4 carbons could be observed. Neopentane does not exhibit a parent peak so it was not necessary to scan through its mass of 72 a.m.u.

The sample used for the LEED/Auger and flash desorption experiments was an iridium (110) single crystal. The crystal was spark cut from a quarter-inch iridium rod after having been oriented by Laue diffractometry. The disc was mechanically polished; the final polish used 0.05μ particle size Linde B alumina. The disc orientation was within $\approx 1°$ of the

(110) crystal face following this preparative procedure.

Materials

The 10 mil iridium wire (Engelhard Industries, Newark, New Jersey) and the single crystal iridium rod (Materials Research Corporation, Orangeburg, New York) were examined by x-ray fluorescence spectroscopy to confirm that they were indeed iridium. The wire sample was found to have trace impurities of iron and rhodium and faint trace impurities of calcium, copper, magnesium, platinum and ruthenium. The materials certification obtained from Materials Research Corporation with the iridium rod indicated the major impurities were 100 ppm ruthenium, 2.5 ppm tungsten and 20 ppm platinum. The other impurities were 10 ppm or less.

The gases used were generally of ultra-high purity. The methane (99.99%), argon (99.9995%) and hydrogen (99.9995%) were obtained from Union Carbide, Linde Division (Chicago, Illinois). The deuterium (99.99%) was purchased from Air Products and Chemicals, Inc. (Los Angeles, California). These gases were purchased in 1 liter glass bulbs with breakseals and were used without further purification. A lecture bottle of neopentane (99.87%) was obtained from Matheson Gas Products (Joliet, Illinois) and was loaded into a glass bulb in a high vacuum system and purified by repeated vacuum distillation using l-N_2. Mass spectral analysis

indicated no observable impurities.

The hydrogen used in the LEED/Auger experiments was taken from a cylinder and purified by passing through a Pd/25% Ag diffuser while the neopentane was used directly from the lecture bottle.

RESULTS AND DISCUSSION

Surface Characterization

LEED, Auger spectroscopy and flash desorption spectroscopy were used to characterize an iridium (110) single crystal surface. LEED and Auger studies were conducted to determine the surface structure and elemental composition while flash desorption studies were used to characterize the surface species.

The (110) single crystal was chosen as a model for the iridium film. A well-sintered thin film is composed principally of low index crystal faces - (100), (110) and (111); a (100) or (111) face could also have served as a film model. The initial Auger spectra indicated that the crystal was contaminated with carbon and oxygen. Oxygen treatment at elevated temperatures has been reported to remove carbon from iridium (110) surfaces (32-34) however in most cases the exact conditions were not reported. It was determined that treatment with oxygen at $P = 5 \times 10^{-6}$ torr and 1100°C for 5 minutes would remove the carbon, and the oxygen could be easily removed after evacuation by continued heating at 1100°C for 20 minutes. If a clean crystal was argon bombarded, a subsequent Auger spectrum would show carbon contamination which indicated that the iridium crystal had a bulk carbon contamination.

One set of experiments which was to be conducted involved determining the reactivity of carbon deposited *via* a neopentane dose with hydrogen. When these experiments were carried out it was found that each time hydrogen was dosed onto the sample the amount of carbon on the surface increased significantly. If a clean sample was dosed with hydrogen for a short period of time (i.e. 1 torr for 120 sec.) and then an Auger spectrum was taken, a large amount of carbon was found to be on the surface. The hydrogen gas used was checked *via* mass spectrometry and no contaminants were found; thus it was concluded that the carbon was diffusing out of the bulk when hydrogen was dosed. This was a major problem since most of the experiments envisioned involved hydrogen doses. After many unsuccessful attempts to obtain a carbon-free sample *via* heating and oxygen or hydrogen treatments, it was decided that the experiments could not be conducted in a manner which would yield useful results.

Iridium exhibits quite a few Auger transitions with peaks at 25, 39, 54, 154, 162, 171, 194, 216, 229, 244, 355 and 380 eV as well as several peaks occurring at energies greater than 550 eV (35). Other transitions of interest occur at 272 eV for carbon and a triplet at 475, 490 and 510 eV for oxygen with the 510 eV peak being the most intense. Since there is no overlap between the iridium and

oxygen or carbon peaks, coverages of oxygen and carbon can be obtained from the relative peak intensities. Figure 4 shows the Auger spectra for a) a clean iridium sample, b) the sample after a 12.5L neopentane dose (1L = 1 langmuir = 10^{-6} torr sec.)and c) after a flash desorption spectrum had been obtained for the sample in b). It was already known that neopentane adsorbs on an iridium thin film at ~468K (as will be discussed later) and thus the increase in carbon in Figure 4(b) is almost certainly due to neopentane adsorption and not due to carbon migration out of the bulk.

Flash desorption spectra were obtained for 4 to 15L doses of neopentane. After the sample had been dosed with neopentane, an Auger spectrum and LEED pattern were obtained, the crystal was flashed and then cooled to 468K so that another Auger spectrum could be taken (all Auger spectra were run at 468K). An increase in the neopentane dose resulted in an increase in the amount of carbon on the surface as indicated by the C(271eV)/Ir(229eV) peak height ratio until the surface was saturated at a dose of approximately 7L.

Figure 5 shows the (1x2) LEED pattern obtained from a clean iridium (110) crystal and the (1x1) pattern obtained from a carbon covered surface. The clean iridium (110) - (1x2) LEED pattern is well-documented and is due to reconstruction of the surface as explained by several models of

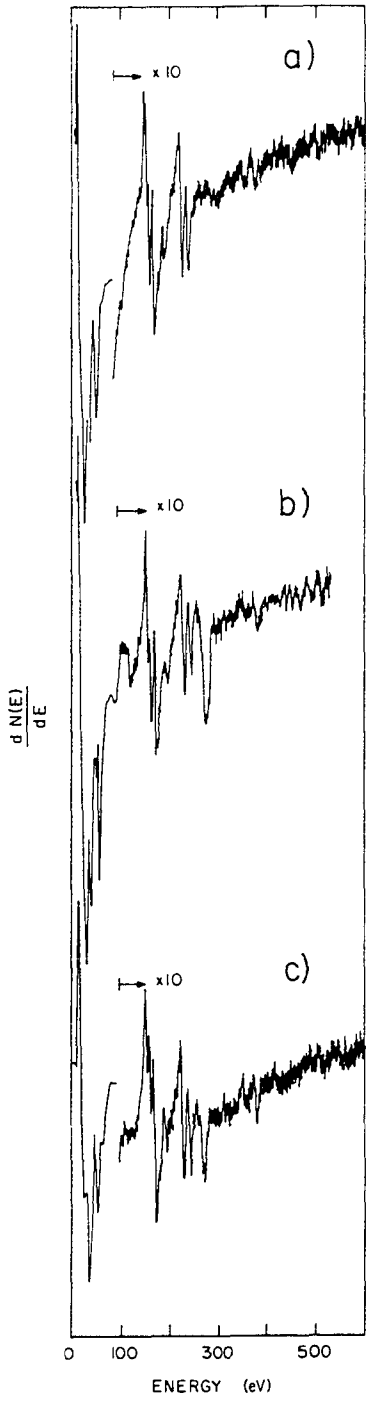

Figure 4. The interaction of neopentane and iridium a) clean iridium sample, b) after exposure to 12.5L neopentane dose, c) sample in (b) after flash desorption experiment.

a)

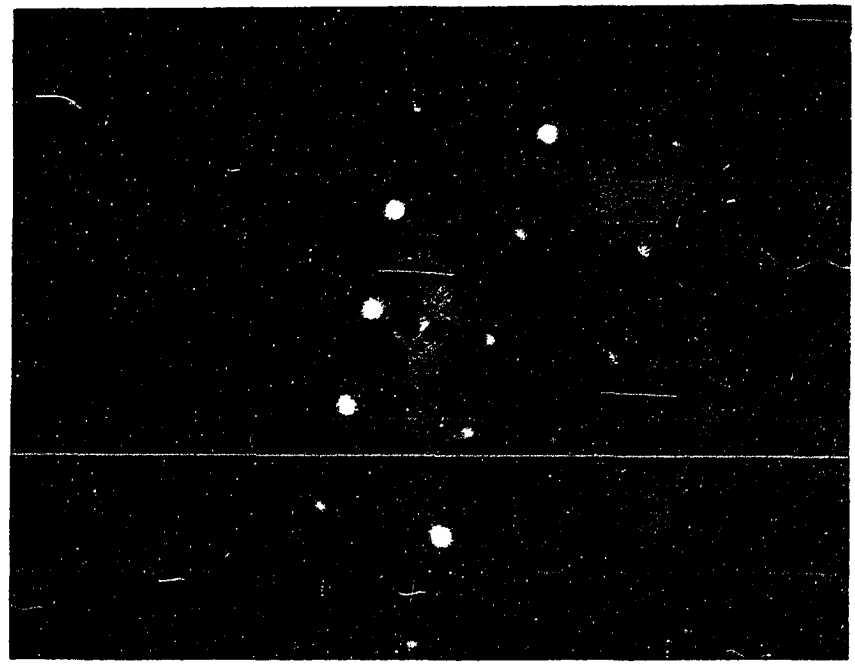

b)

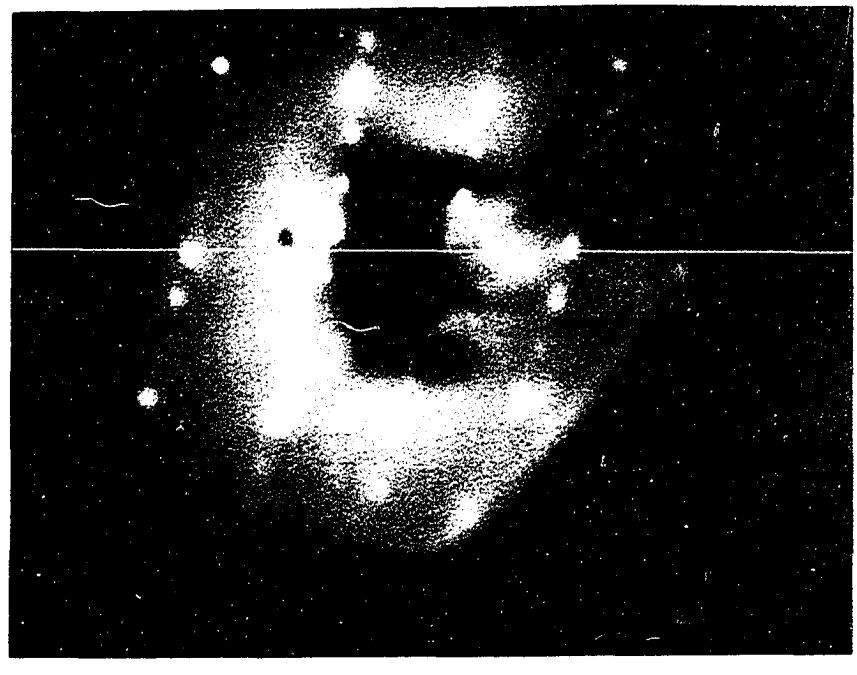

Figure 5. LEED patterns obtained from a (110) iridium single crystal: a) (1x1) pattern for a carbon contaminated surface; b) (1x2) pattern for a clean surface.

which the missing row model is most plausible (32,33). Small carbon contaminants have been found to stabilize the Ir (1x1) structure (32,36) and thus the (1x1) pattern which results from the neopentane adsorption is probably due to the stabilization of the unreconstructed surface and not the formation of an ordered carbon overlayer.

When the crystal, after being exposed to various neopentane doses at 468K, was heated to 1373K in front of the ionizer of the mass spectrometer, the only desorption products observed were small amounts of carbon monoxide, carbon dioxide and water. These products are undoubtedly being desorbed from the crystal supports, heater block and/or the manipulator which were all heated to various degrees via conductance from the heater. It is not likely that the flash desorption products came from the crystal surface because there was no oxygen on the sample initially. The lack of a hydrogen desorption peak is not surprising because previous results have shown that hydrogen desorption on iridium begins at temperatures <423K (36,37). It is important however that no neopentane or any lower hydrocarbons were desorbed upon heating the sample to 1373K and supports the hypothesis, which will be discussed more later, that neopentane completely dissociates into carbon and hydrogen when it adsorbs on iridium at 468K.

It can be seen by a comparison of Figure 4(b) and (c)

that the amount of carbon on the surface is lower after the flash desorption than prior to it. Since no carbon is desorbed from the surface, the reduction is most likely due to carbon diffusion into the bulk.

Thin Film Characterization

The thin films deposited by evaporation from a wire were observed to be of uniform thickness and distributed over the entire surface of the round bottom flask. The thickness of these films could be estimated by several different methods. One method was based on the rate of evaporation W in units of grams of iridium per square centimeter per second as expressed by the following equation:

$$\log W = 9.98 - 0.5 \log T(K) - 31320\ T(K)^{-1} \qquad (38)$$

The deposition temperature for film #10 was estimated with an optical pyrometer to be 2200K and this results in an evaporation rate of 1.18×10^{-6} gms-cm^{-2}-sec.$^{-1}$. The film was deposited over a period of 40 minutes from a wire with a surface area of 0.64 cm^2; thus 1.81×10^{-3} gms of iridium was deposited over the 250 cm^2 surface of the reaction cell. If the density of the film is assumed to be the same as the iridium bulk density, 22.4 gm-cm^{-3} (39), then a film thickness of 34Å was calculated. The second method was based on the difference in the weight of the iridium wire before and after film deposition. Again assuming that the film is

evenly distributed and has the same density as bulk iridium the thickness of film #10 was found to be 28.9Å. The difference in film thickness as determined by these two methods is small and can be attributed to error in measuring the temperature used in the first method and to weight changes due to the spotwelding of the wire to the leads in the later method. A third method involves the variation in the amount of hydrogen adsorbed with the film thickness as determined by Masterson (40). The film thickness was found to be directly proportional to the surface area of the films which was measured by hydrogen adsorption for films with thicknesses in the range 30-300Å. Although the films used in this study are at the lower limit of film thicknesses studied by Masterson, the amount of hydrogen adsorbed indicated a film thickness of approximately 30Å.

The number of surface sites for each film had to be determined in order to convert the rates from units of torr/sec. to molecules/site/sec. Several different methods exist for determinine the surface area of a catalyst, however the BET method using argon or nitrogen as the adsorbing gas is by far the most popular (41,42). Since iridium has not been studied very extensively as a catalyst, there are few studies in which the surface area of iridium has been measured. Of these, various gases, hydrogen (5,11,43,44) and oxygen (5), have been chemisorbed and then the number of

sites were determined from the number of adsorbed species. The surface area was then usually determined by assuming the number of surface metal atoms and estimating the number of metal atoms/cm^2. The determined surface area, however, may not be correlated to the active surface area; for instance, the surface area determined by hydrogen adsorption which would assume monoadsorption, would differ from the active surface area for hydrogenolysis if the hydrocarbon adsorbs only on a site composed of several metal atoms.

In this work the number of active surface sites was determined from the amount of methane which was desorbed from the surface (after exposure to neopentane) by reaction with hydrogen. The number of surface sites was not correlated to the number of surface atoms which would require assuming the number of surface atoms involved in each site. Figure 6 shows the amount of methane produced during a hydrogen flush with P_{H_2} = 0.200 torr plotted against the amount of hydrogen dosed into the cell during the prior kinetic run. Thus after each run in a series of kinetic runs at 468K in which the neopentane pressure was held constant at 1.6×10^{-3} torr and the hydrogen pressure was varied, the cell was dosed with 0.200 torr hydrogen and the methane production was monitored. It is seen that the maximum amount of methane produced is obtained from the y-intercept at which point the hydrogen pressure is zero. It is

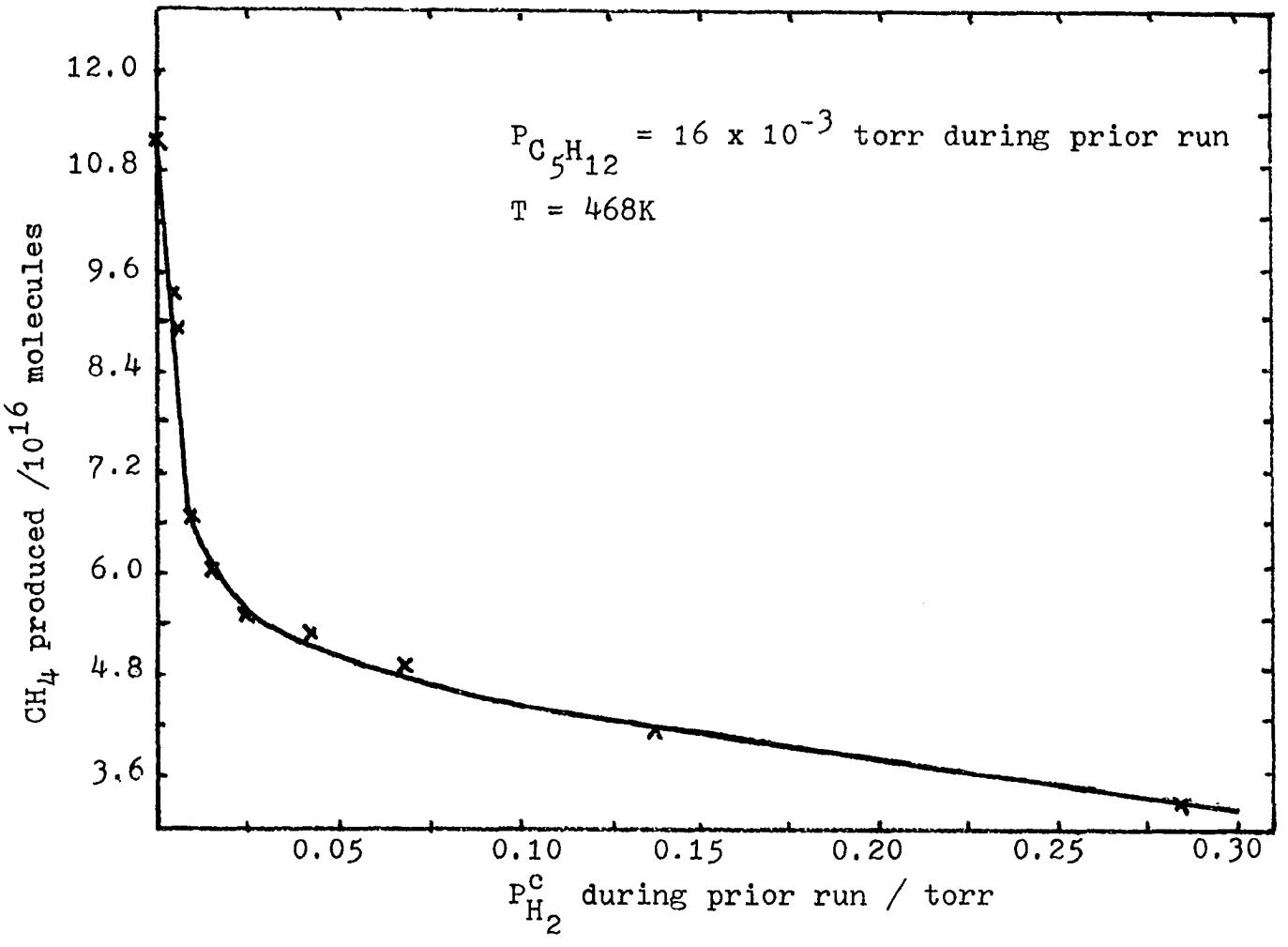

Figure 6. The variation in the methane produced during a 0.200 torr hydrogen flush with the pressure of hydrogen in the cell during the kinetic run prior to the flush.

also possible to calculate the number of active sites from the methane production during the hydrogen flushes between each run in a set of kinetic runs made at a constant hydrogen pressure as shown in Figure 7. In this case 0.200 torr hydrogen was dosed into the cell between the kinetic runs conducted under the following conditions: $P_{C_5H_{12}}$ = (1 - 50) x 10^{-3} torr, P_{H_2} = 28 torr and T = 468K.

The amount of methane produced from the different films varied from (1 - 10) x 10^{16} molecules. It was found that there were more active sites present on films deposited at room temperature and subsequently sintered at 483K than on the films deposited at the sintering temperature. The reaction rates at similar conditions (expressed as turnover numbers), the product distributions and the order of the reaction with respect to the partial pressures of neopentane, hydrogen and methane were the same regardless of the film used, which indicates that the same mechanism is involved on the different films which therefore differ only in the amount of active surface area.

The variation in the number of active sites could have several origins. The surface deposited at room temperature may be composed of more crystallites with the necessary properties for the dissociative adsorption of neopentane. This may mean that it contains more crystallites with desirable crystal faces exposed or for that matter a certain crystal

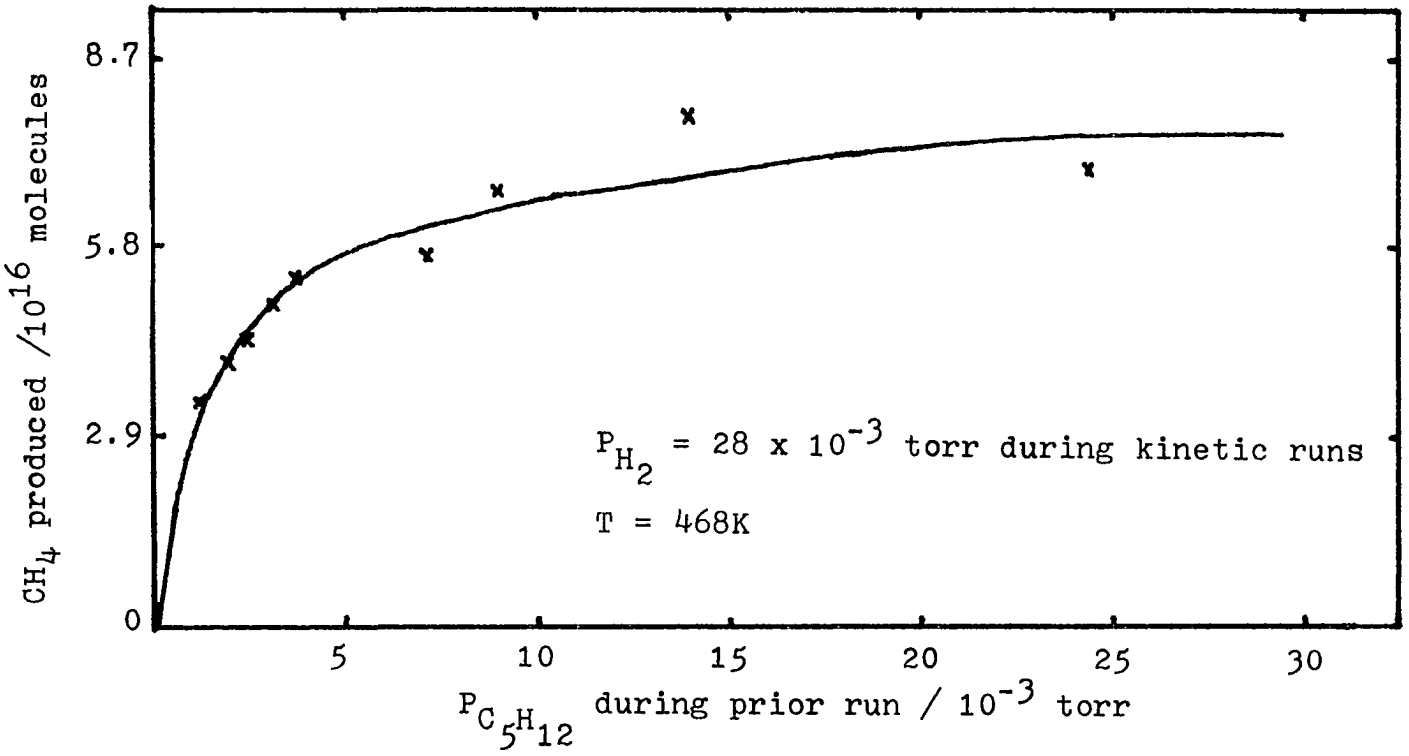

Figure 7. The variation in the methane produced during a 0.220 torr hydrogen flush with the change in the pressure of neopentane in the cell during the kinetic run prior to the flush.

face which is inactive for hydrocarbon adsorption may be more prevalent in the films deposited at high temperature. It has been proposed that (111) crystal faces are inactive toward hydrogenolysis reactions (45-47) and it may be that more (111) crystal faces are exposed on the more highly sintered films. This would be expected because the (111) face is the most densely packed face in the fcc metals, and hence atoms on this face are missing the smallest number of neighbors. Thus it would be expected to have the lowest surface energy/cm^2. Sintering would tend to move the system toward equilibrium, developing preferentially those faces of lowest energy. Another very plausible explanation is that the less sintered films contain more kinks and steps in the surface. These surface imperfections have been proposed in the past as the active sites for hydrogenolysis (48-51).

Difficulties Encountered in Conducting Kinetic Experiments

The bulk of the data collected on the neopentane - hydrogen system was collected in the ultra high vacuum system previously described. The results obtained consist mainly of kinetic order data but also include the neopentane adsorption studies and deuterium exchange studies. Before discussing the results per se, several topics will be discussed which tended to obscure the true kinetics.

As mentioned in the experimental section, all rates were converted from units of mv/sec. to torr/sec. with mass spectrometer sensitivities. One might expect these sensitivities to vary slightly from day to day due to electronic aging of the components of the mass spectrometer, however for any one species the sensitivity should remain constant when the pressures of other compounds with nonoverlaping spectra are varied. There seemed to be a problem here however, for when methane was dosed into the reaction cell at 473K with varying pressures of hydrogen, the methane sensitivity as measured by the peak at m/z = 16 varied as shown in Figure 8. These sensitivity results were very reproducible and originally they were believed to be true sensitivities and their variations ascribed to changes in background pressure affecting either the flow of methane through the leak valve or the actual response of the mass spectrometer. After much reflection on these hypotheses it was decided that neither was tenable. Molecular flow through an orifice is dependent on the molecular weight of the gases passing through it, but is inversely proportional to the square root of the molecular weight and consequently a molecular flow effect on the sensitivity would be in a direction opposite to that actually observed. The flow through the leak to the mass spectrometer is actually not dependent on the molecular weights of the components in the

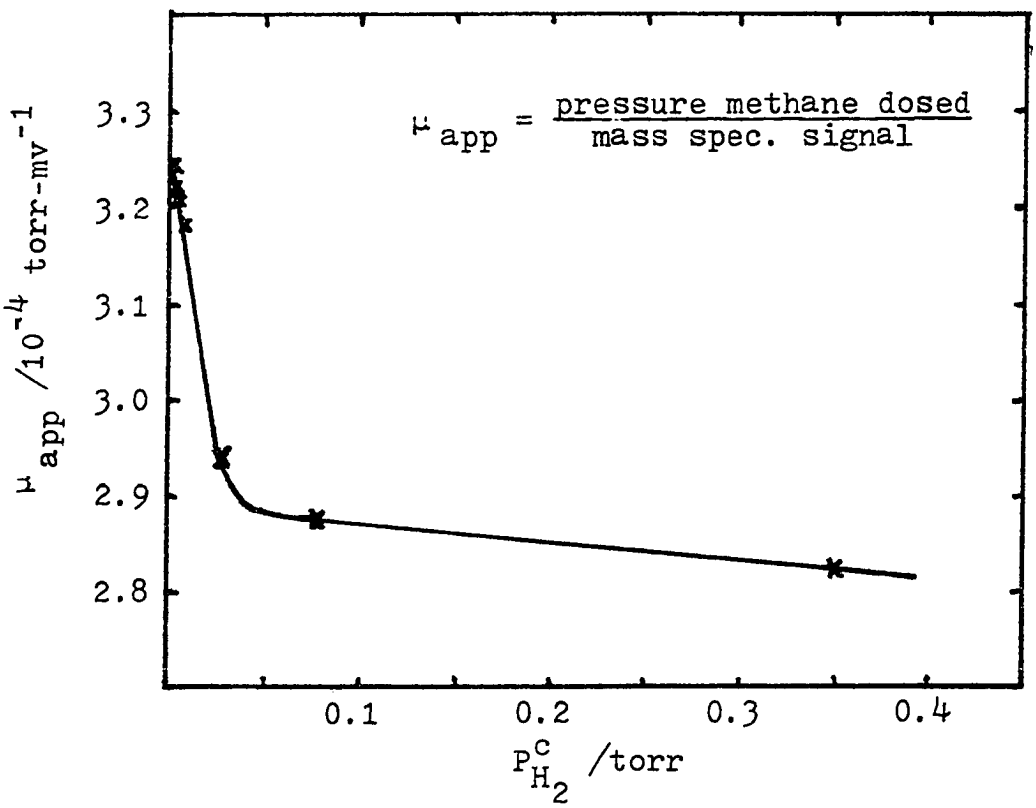

Figure 8. The apparent methane sensitivity at varying pressures of hydrogen in the reaction cell.

gas mixture. The other hypothesis had to be discarded because the mass spectral output for one m/z ratio cannot be affected by the change in other m/z ratios as is obvious from the previous discussion on the mass spectrometer. The only possible effect would be saturation of the multiplier and again this would not affect any peaks except the one actually saturating the multiplier. Another explanation had to be found and it turns out that the sensitivity was not really changing, instead the pressure of methane was varying even though a constant pressure of methane had been dosed into the reaction cell. A portion of the methane (the amount depended on the hydrogen pressure) was adsorbed on the iridium film and consequently the actual pressure of methane was smaller than the pressure of methane measured by the capacitance manometer by the amount adsorbed on the iridium film. The following model can be derived assuming that: methane dosed in (P_{app}) = methane in gas phase in reactor (P_{CH_4}) + methane adsorbed and the following equilibria.

$$CH_4 + 2* \underset{}{\overset{K_2}{\rightleftharpoons}} CH_3* + H* \qquad (2)$$

$$H_2 + 2* \underset{}{\overset{K_3}{\rightleftharpoons}} 2H* \qquad (3)$$

Using the conservation of sites and the above equilibria

$$(CH_3*)(H*) = K_2 P_{CH_4}(1 - CH_3* - H*)^2 \qquad (4)$$

$$(H^*)^2 = K_3 P_{H_2} (1 - CH_3^* - H^*)^2 \tag{5}$$

so

$$\frac{(CH_3^*)}{(H^*)} = \frac{K_2 P_{CH_4}}{K_3 P_{H_2}} \tag{6}$$

$$(H^*) = \frac{K_2 P_{H_2}}{1 + (K_3 P_{H_2})^{\frac{1}{2}} + \frac{K_2 P_{CH_4}}{(K_3 P_{H_2})^{\frac{1}{2}}}} \tag{7}$$

$$(CH_3^*) = \frac{K_2 P_{CH_4}}{(K_3 P_{H_2})^{\frac{1}{2}} + K_3 P_{H_2} + K_2 P_{CH_4}} \tag{8}$$

Then

$$\frac{P_{app} V}{RT} = \frac{P_{CH_4} V}{RT} + \frac{n_m K_2 P_{CH_4}}{(K_3 P_{H_2})^{\frac{1}{2}} + K_3 P_{H_2} + K_2 P_{CH_4}} \tag{9}$$

where n_m is the number of moles in a monolayer. Let μ = mass spec. signal/P_{CH_4}, and $\mu_{app} = (P_{CH_4}/P_{app})$. Then

$$\mu_{app} = \mu \left\{ 1 + \frac{n_m K_2 RT}{V} \left((K_3 P_{H_2})^{\frac{1}{2}} + K_3 P_{H_2} + K_2 P_{CH_4} \right)^{-1} \right\} \tag{10}$$

rearranging

$$\frac{\mu}{\mu_{app} - \mu} = \frac{V}{n_m K_2 RT} \left\{ (K_3 P_{H_2})^{\frac{1}{2}} + K_3 P_{H_2} + K_2 P_{CH_4} \right\}^{-1} \tag{11}$$

The model illustrated by equation (11) can be compared to the sensitivity results. At low hydrogen pressures the first order term in hydrogen will be small compared to the

square root term and thus $\frac{\mu}{\mu_{app} - \mu}$ plotted against $(P_{H_2})^{\frac{1}{2}}$ should yield a straight line with slope $\frac{V}{n_m RT} \frac{K_3^{\frac{1}{2}}}{K_2}$ and y-intercept $\frac{V}{n_m RT} P_{CH_4}$ (at $P_{H_2} = 0$). Figure 9 is such a plot with a slope of 30 $torr^{-\frac{1}{2}}$ and intercept of 2.9. At $P_{H_2} = 0$ the pressure of methane in the gas phase was 2.91×10^{-3} torr and consequently $n_m = 6.27 \times 10^{-8}$ moles or 3.77×10^{16} molecules and $(K_3)^{\frac{1}{2}}/K_2 = 3.02 \times 10^{-2}$ $torr^{-\frac{1}{2}}$. The number of moles in a monolayer can also be calculated from Figure 8 and equation (10) whereby at zero hydrogen pressure

$$\frac{\mu}{\mu_{app}} = \frac{RT}{V} n_m$$

This method yields a value of $n_m = 4.19 \times 10^{-8}$ moles which agrees reasonably well with 6.27×10^{-8} moles. The values for n_m agree very well with the number of active surface sites determined to be $(1 - 10) \times 10^{16}$ from the amount of methane produced by reaction with hydrogen as discussed previously. It thus appears that the above model adequately explains the observed sensitivity data. From equation (10) it is seen that $\mu_{app} \rightarrow \mu$ at either high hydrogen or neopentane pressure.

Expansion curves, as previously mentioned in the Experimental Section, were used to calculate the pressure of a gas in the reaction cell after expansion from the manifold where the pressure of the gas had been measured by the capacitance

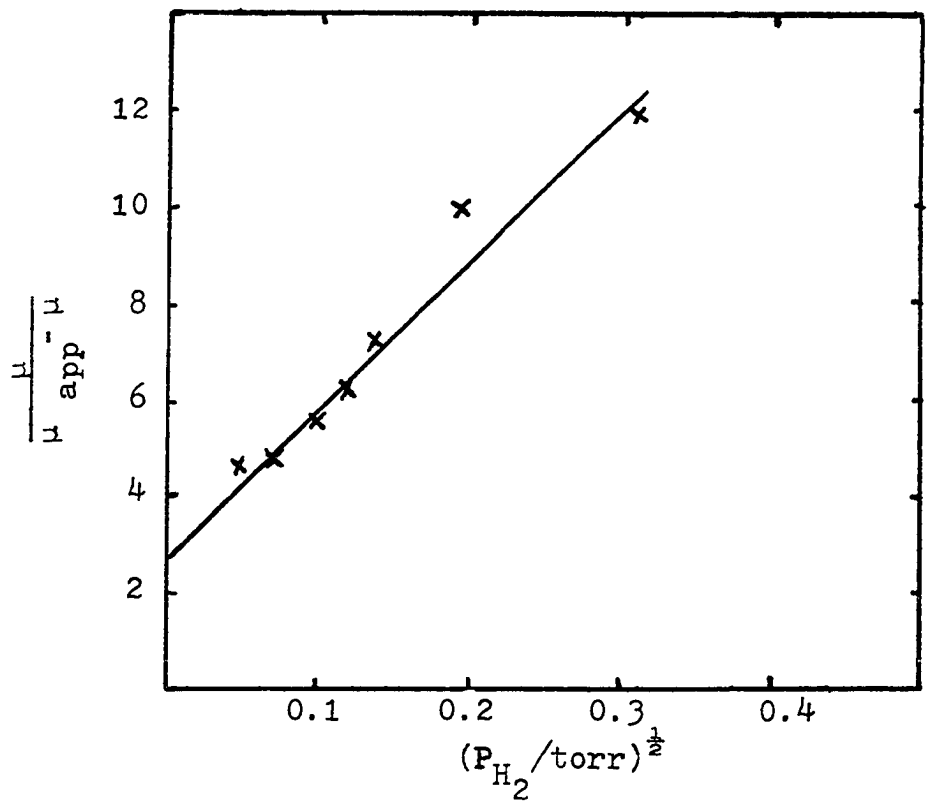

Figure 9. The fit of the sensitivity data to equation (11).

manometer. No problems were encountered in obtaining expansion factors for hydrogen, but neopentane gave difficulties. After expanding neopentane of a known pressure into the reaction cell, the pressure as determined by the capacitance manometer decreased and then increased often leveling off to indicate a higher final pressure than initial. It was determined by monitoring the mass spectral output that a good deal of hydrogen was produced and after a while a small amount of methane was produced, indicating that neopentane adsorbs on the iridium catalyst dissociatively leading to hydrogen desorption. The possibility that the hydrogen desorbing was actually preadsorbed hydrogen remaining on the surface from the prior hydrogen flush was considered. There are studies in which the flash desorption spectrum of hydrogen on iridium has been reported which show that at $\sim$473K no hydrogen should remain adsorbed on the surface (37,38,52). A very simple experiment was nevertheless performed to unequivocally clarify the origin of the hydrogen. The iridium catalyst was flushed with deuterium, evacuated and then neopentane was dosed into the cell. Hydrogen (and not deuterium) was produced, resulting therefore unambiguously from the dissociative adsorption of neopentane. Knowledge of the amount of hydrogen produced compared to the amount of neopentane adsorbed allows a determination of the extent of carbon-hydrogen bond breakage during adsorption. The

analysis of several experiments reveals that the adsorption of each neopentane molecule was accompanied by the liberation of five to eight molecules of hydrogen. Of course the maximum possible value for this ratio is only six and the cause for the large error found in these calculations is due to the difficulty in determining the actual amount of neopentane which has adsorbed onto the catalyst. After determining the ratio using several methods to calculate the amount of adsorbed neopentane, the conclusion has been reached that the adsorbed intermediate is highly dissociated and contains no greater than two hydrogen atoms; that is, the surface composition is C_5H_{0-2}. This is not the first time such a highly dissociated intermediate has been proposed, in fact as far back as 1958 Wright et al. (53) reported the following compositions for methane and/or ethane: CH_2 at 373K and C_2H_2 at 363K on tungsten, CH_{0-1} on nickel and CH_2 on iron at 473K. Ross et al. (54) reported the following results: a)on tungsten neopentane adsorbed as C_5H_8 at 373K, propane as C_3H_5 at 293-423K and methane as CH_2 at 294K and b)on palladium neopentane adsorbed as C_5H_{10} at 293K, C_5H_8 at 373K and C_5H_7 at 453K. Anderson and Baker (8) reported hydrogen to carbon ratios for adsorbed ethane and propane residues on nickel, tungsten, rhodium and platinum films at various temperatures between 395 and 563K as being between 0.4 and 2.4 depending on the hydrocarbon and

and catalyst. Sárkány and Tétényi (55) recently reported the hydrogen to carbon ratio for ethane residues at 483K to be 0.25 and 0.33 on nickel and cobalt respectively and between 1 and 2 on rhodium, palladium and platinum. Somewhat higher values were reported at 428K. This meager sampling of studies shows that highly dissociated residues of various hydrocarbons have been observed in the past and the degree of dissociation is dependent on the metal, temperature and hydrocarbon involved.

The observation that a few millitorr of hydrogen were liberated by the adsorption of neopentane was used to clarify the unusual hydrogen order dependence shown by the x's in Figure 10. These results were obtained at 467K at a neopentane pressure which varied from (0.99 to 1.6) x 10^{-3} torr and hydrogen pressures (dosed into the cell) in the range (0.25 to 63) x 10^{-3} torr. At very low hydrogen pressures, the order of the reaction went to zero which would be quite difficult to explain in terms of a mechanism since at higher hydrogen pressures the order is positive. It turns out that when the hydrogen pressure dosed into the reaction cell is increased by the amount which comes from the neopentane adsorption, the hydrogen order plot has a positive slope even at the lowest hydrogen pressures as indicated by the c's in Figure 10. The actual hydrogen cell pressure was calculated from the mass spectrometer output instead of

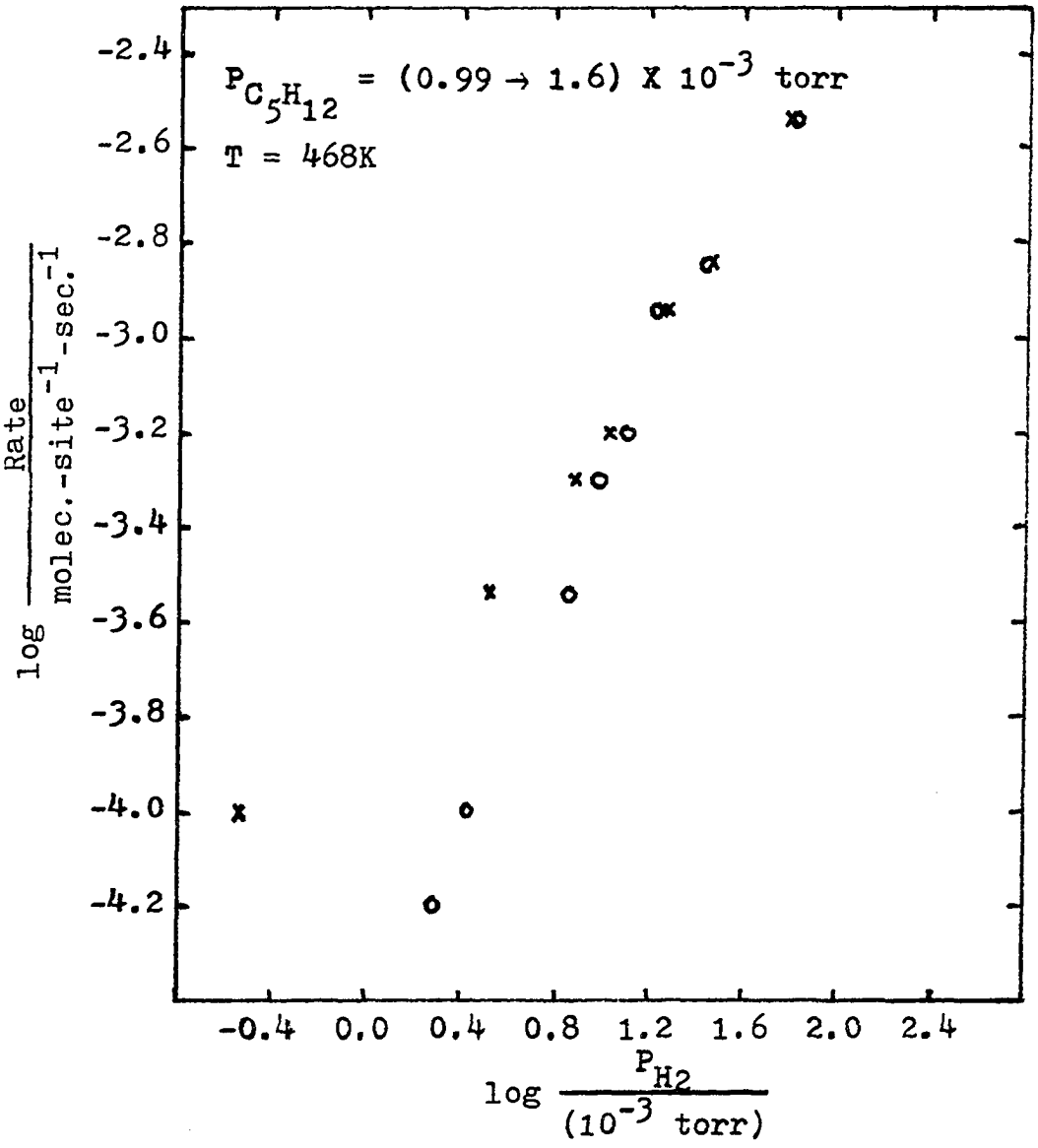

Figure 10. A hydrogen order plot illustrating the difference when the hydrogen pressure is obtained from the mass spectrometer output (o's) and from the expansion of a known pressure from the manifold (x's). The o at the lowest hydrogen pressure has no corresponding x because no hydrogen was dosed into the manifold for that run.

using the capacitance manometer output which represented only the amount of hydrogen dosed into the cell and did not take into account that which originated from the neopentane adsorption. It should be noted that although the neopentane pressure dosed into the reaction cell was constant (as was the case for all hydrogen order plots) the actual pressure of neopentane in the cell varies as the hydrogen pressure varies because of the competition for sites. Thus, whenever very low pressures ($<10 \times 10^{-3}$ torr) of either neopentane or hydrogen were involved, the mass spectral output was used to determine the actual pressure of the reactant in the cell.

Results of Kinetic and Deuterium Exchange Experiments

All of the results were obtained on five films which were found to exhibit rates which were reproducible to within ±10% from day to day and film to film. Each film was used until it was necessary to replace it due to modification of the system, break-down or anytime when it was necessary to bring the reaction cell up to atmospheric pressure. The film was stored in 1 torr hydrogen at room temperature when experiments were not in progress. The amount of methane produced was monitored every 5 seconds for two to three minutes. No induction period was observed before methane formation began; however, the first two or three data points

were always ignored because it took several seconds for the gases to equilibrate across the leak. The reaction conversions were 1 to 2% and loss through the leak after three minutes was approximately 5%. The reaction therefore took place in a static reactor and the observed rates were initial rates. Approximately five times as much methane was produced as neopentane consumed, confirming that methane was the only hydrogenolysis product. The film was "cleaned" of reactive carbon after each run by exposing it to hydrogen for three or four minutes. If this was not done, the observed rate in the next run was found to be lower than if the surface had been "cleaned".

Reaction orders with respect to the partial pressures of neopentane, hydrogen and methane were determined at temperatures in the range 443 to 468K. Pressure ranges investigated were the following: neopentane (1 to 400) x 10^{-3} torr, hydrogen (20 to 3,000) x 10^{-3} torr and methane (0.32 to 25) x 10^{-3} torr. The reaction order with respect to the partial pressure of neopentane varied from +0.95 to -0.80 as the neopentane pressure was increased. The hydrogen reaction order varied from +2.0 to -0.1; the hydrogen partial pressure could not be increased above 3 torr because of limits imposed by the capacitance manometer and so a (presumed) limiting negative order in hydrogen was not documented. The methane order was -0.03 or essentially zero.

The order plots are shown in the next section along with the fit to the proposed mechanism.

The activation energy was determined from an Arrhenius plot of lnR versus 1000/T obtained at $P_{C_5H_{12}} = 6.2 \times 10^{-3}$ torr and $P_{H_2} = 0.197$ torr over the temperature range 400 to 473K as shown in Figure 11. The data were collected by increasing the temperature in increments, measuring the rate (x's) after the temperature had stabilized at the new temperature; the reaction cell was then cooled down to 400K and the rate was measured again and then at a slightly higher temperature with these results indicated by the o's in Figure 11. The good fit of the o's with the original data indicates that the surface did not undergo additional sintering at the higher temperatures and that the data were reproducible. The slope of the plot is $-E_{act}/1000R$ and yields an apparent activation energy of 17.6 kcal/mole over the temperature range studied. This is the activation energy resulting from a rate expression which involves products and quotients of rate constants and not necessarily the activation energy for any one step in the mechanism. The only activation energies reported for iridium were between 46 and 60 kcal/mole and were obtained over supported catalysts at total pressures >10 torr (5,11); the reaction conditions and product distributions for those studies differed markedly from those in the present work.

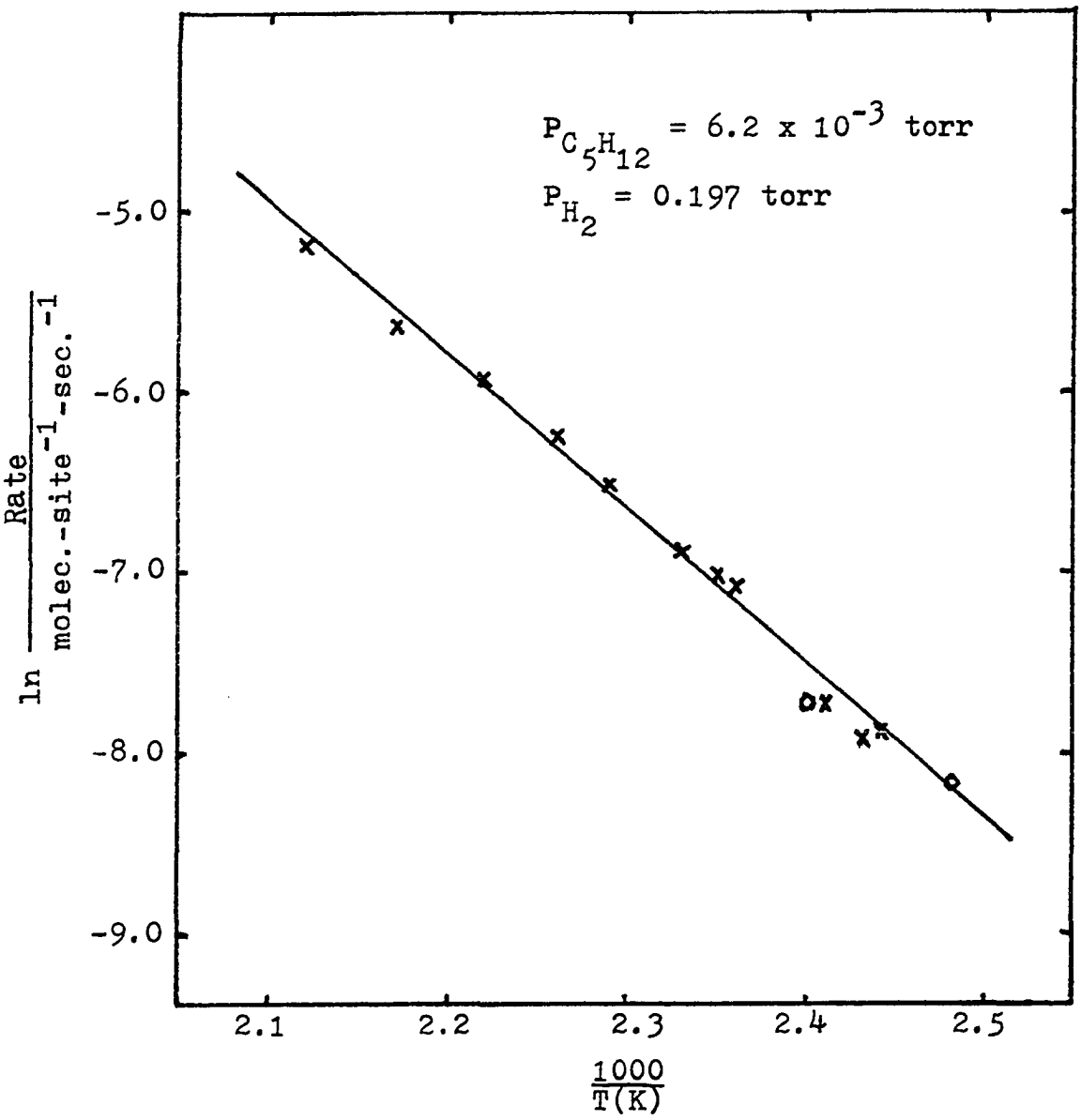

Figure 11. Temperature dependence for the hydrogenolysis of neopentane on an iridium film.

Deuterium was used instead of hydrogen in order to determine if any reversible adsorption of neopentane could be detected. The only additional peaks observed in the mass spectra occurred at m/z ratios of 17-20 and correspond to the four deuterated methane species. A large portion of the product was perdeuteromethane which tends to indicate either extensive dissociation of the carbon fragments on the surface or very rapid exchange between the hydrocarbon fragments and deuterium. The absence of neopentane exchange supports the hypothesis that neopentane chemisorption is irreversible under the conditions at which this study has been made. Ethane exchange has been observed under hydrogenolysis conditions by Mahaffy and Hansen (27) on iridium films which might suggest that the hydrogenolysis of ethane involves reversible adsorption; however, Martin (45,46) has proposed that two types of ethane species are adsorbed on Ni/SiO_2 catalysts, one of which is reversibly adsorbed and the other one, the hydrogenolysis intermediate, is irreversibly adsorbed. Boudart (56) has proposed a mechanism for the hydrogenolysis of ethane which involves irreversible ethane adsorption. This question has not been addressed for neopentane; however, as previously discussed, exchange products have been observed simultaneously with deuterolysis products over various catalysts (13-15).

Mechanistic Considerations

The kinetics of a reaction often fit a very simple rate law of the form shown in equation (1) where the order with respect to the partial pressure of both reactants is constant. This simplistic analysis of reaction kinetics is not possible for the neopentane hydrogenolysis results obtained in this study because the reaction orders varied with respect to both reactants. Two classical models often invoked to explain rate laws with varying reaction orders, the Rideal-Eley and Langmuir-Hinshelwood mechanisms, will be reviewed quickly here.

The Rideal-Eley mechanism involves the reaction between a gas-phase molecule and an adsorbed species, as indicated by the following equations, where * is a surface site, A* is an A molecule chemisorbed on the surface, K_{12} is the equilibrium constant and k_{13} is a rate constant.

$$A(g) + * \underset{}{\overset{K_{12}}{\rightleftharpoons}} A* \qquad (12)$$

$$A* + B(g) \xrightarrow{k_{13}} AB(g) + * \qquad (13)$$

The overall reaction is

$$A(g) + B(g) \overset{K}{\rightleftharpoons} AB(g) \qquad (14)$$

The rate equation for this reaction can be written

$$\text{Rate} = k_{13}(A*)P_B \qquad (15)$$

The fractional surface coverage of A can be determined from

the reaction equilibrium involved in equation (12) and the number of surface sites (*) can be determined from the total number of surface sites as follows:

$$(A^*) = K_{12}P_A(*) \tag{16}$$

$$(*) = \frac{1}{1 + K_{12}P_A} \tag{17}$$

The rate is then

$$\text{Rate} = \frac{k_{13}K_{12}P_BP_A}{1 + K_{12}P_A} \tag{18}$$

The order of the reaction with respect to the adsorbed species is +1 to 0 with increasing P_A and with respect to reactant B is +1 at all pressures of B. Rideal-Eley kinetics, which also apply when one of the reactants is physisorbed on a chemisorbed layer of the other reactant, thus always exhibits constant +1 reaction order for one of the reactants and the other one varies from +1 to 0 as the reactant pressure is increased.

The Langmuir-Hinshelwood mechanism involves the reaction of two adsorbed species which are competing for the same sites, where the overall reaction is the same as used in the derivation above as shown in equation (14). In this case the following equilibria are involved:

$$A(g) + * \underset{}{\overset{K_{19}}{\rightleftharpoons}} A^* \tag{19}$$

$$B(g) + * \underset{}{\overset{K_{20}}{\rightleftharpoons}} B^* \tag{20}$$

$$A^* + B^* \xrightarrow{k_{21}} AB + 2^* \tag{21}$$

The rate is expressed by

$$\text{Rate} = k_{21}(A^*)(B^*) \tag{22}$$

Assuming that the equilibria of reactions (19) and (20) are rapidly attained and that surface sites are conserved, the following equations can be derived:

$$(A^*) = K_{19}P_A(^*) \tag{23}$$

$$(B^*) = K_{20}P_B(^*) \tag{24}$$

$$(^*) = \frac{1}{1 + K_{19}P_A + K_{20}P_B} \tag{25}$$

so that

$$\text{Rate} = \frac{k_{21}K_{19}K_{20}P_AP_B}{(1 + K_{19}P_A + K_{20}P_B)^2} \tag{26}$$

The reaction orders with respect to either reactant obtained from the rate law shown in equation (26) vary from +1 to -1 as the pressure of the reactant of interest is varied from low to high pressures.

To summarize, the Rideal-Eley mechanism results in constant first order kinetics with respect to the partial pressure of one reactant and +1 to 0 order dependence on the pressure of the other; the Langmuir-Hinshelwood mechanism exhibits +1 to -1 orders with respect to the partial pressures of both reactants. Either rate law will simplify to

the constant reaction order case if the fractional surface coverages of the adsorbed species are very small - in which case the denominators in the rate laws in equations (18) and (26) will be 1.

Since the order of the reaction with respect to the partial pressures of both neopentane and hydrogen vary from a positive to a negative order as the partial pressures are increased, it was decided that a Langmuir-Hinshelwood type mechanism should be used to explain the kinetics. On the basis of the neopentane adsorption experiments, which indicated that neopentane is highly dissociated upon adsorption, it was decided to try to fit the kinetic results by using a mechanism involving the irreversible, dissociative adsorption of neopentane, the reversible dissociative adsorption of hydrogen and subsequent hydrogenation of the carbon fragments as shown below.

$$H_2 + 2* \rightleftharpoons 2H* \qquad (27)$$

$$C_5H_{12} + 2* \longrightarrow C_5H_{11}* + H* \qquad (28)$$

$$C_5H_{11}* + * \longrightarrow C_5H_{10}* + H* \qquad (29)$$

$$C_5H_{10}* + * \longrightarrow C_5H_9* + H* \qquad (30)$$

$$C_5H_9* + * \longrightarrow C_4H_9* + C* \qquad (31)$$

$$C_4H_9* + * \longrightarrow C_4H_8* + H* \qquad (32)$$

$$C_4H_8* + * \longrightarrow C_4H_7* + H* \qquad (33)$$

$$C_4H_7^* + * \longrightarrow C_4H_6^* + H^* \quad (34)$$

$$C_4H_6^* + * \longrightarrow C_3H_6^* + C^* \quad (35)$$

$$C_3H_6^* + * \longrightarrow C_3H_5^* + H^* \quad (36)$$

$$C_3H_5^* + * \longrightarrow C_3H_4^* + H^* \quad (37)$$

$$C_3H_4^* + * \longrightarrow C_3H_3^* + H^* \quad (38)$$

$$C_3H_3^* + * \longrightarrow C_2H_3^* + C^* \quad (39)$$

$$C_2H_3^* + * \longrightarrow C_2H_2^* + H^* \quad (40)$$

$$C_2H_2^* + * \longrightarrow C_2H^* + H^* \quad (41)$$

$$C_2H^* + * \longrightarrow C_2^* + H^* \quad (42)$$

$$C_2^* + * \longrightarrow 2C^* \quad (43)$$

$$C^* + H^* \rightleftharpoons CH^* + * \quad (44)$$

$$CH^* + H^* \rightleftharpoons CH_2^* + * \quad (45)$$

$$CH_2^* + H^* \rightleftharpoons CH_3^* + * \quad (46)$$

$$CH_3^* + H^* \rightleftharpoons CH_4 + 2^* \quad (47)$$

Each of the above steps has a corresponding rate or equilibrium constant which will have a subscript corresponding to the equation number. Steps shown in equations (28) through (43) are proposed only as one possible pathway to accomplish the overall reaction

$$C_5H_{12} + 17^* \longrightarrow 5C^* + 12H^* \quad (48)$$

<u>via</u> bimolecular reactions.

The rate law for this reaction mechanism can be derived either by using the steady state approximation or a steady flow method. The latter method will be shown below.

$$R = \text{Rate} = -\frac{dC_5H_{12}}{dt} = k_{28}P_{C_5H_{12}}(*)^2 \qquad (49)$$

The equation for the coverage of sites in terms of constants and the pressures of neopentane and hydrogen must be derived in order to make the above rate equation useful. The steady flow of carbon throughout the reaction requires that

$$\frac{dCH_4}{dt} = 5R = 5k_{28}P_{C_5H_{12}}(*)^2 \qquad (50)$$

since five methanes are produced for each neopentane molecule consumed. Equation (50) is related to the concentration of the adsorbed species involved in the reactions shown in equations (44) - (47) as follows where the adsorption of the methane produced is assumed negligible.

$$\frac{dCH_4}{dt} = 5R = k_{47}(CH_3*)(H*) \qquad (50a)$$

$$= k_{46}(CH_2*)(H*) - k_{-46}(CH_3*)(*) \qquad (50b)$$

$$= k_{45}(CH*)(H*) - k_{-45}(CH_2*)(*) \qquad (50c)$$

$$= k_{44}(C*)(H*) - k_{-44}(CH*)(*) \qquad (50d)$$

The sum of the terms on the right reflects the net consumption of H*, and hence is 20R. The net rate of supply at steady state equilibrium is

$$12R + 2k_{27}P_{H_2}(*)^2 - 2k_{-27}(H^*)^2 = 20R \qquad (51)$$

thus

$$(*)^2 = \frac{k_{-27}(H^*)^2}{k_{27}P_{H_2} - 4k_{28}P_{C_5H_{12}}} \qquad (52)$$

Any term which may be negative must be regarded with suspicion because the rate, of course, cannot be negative. From equations (50) and (52) it is evident that $k_{27}P_{H_2} - 4k_{28}P_{C_5H_{12}} = k_{-27}(H^*/*)^2$, is a positive number so that the denominator in equation (52) can never be zero or negative.

Equation (52) can be used with equations (50-50d) to determine the surface coverages of (CH_3^*), (CH_2^*), (CH^*) and (C^*) in terms of the coverages of empty surface sites, pressures of neopentane and hydrogen and rate constants.

$$(CH_3^*) = \frac{5k_{28}k_{-27}^{\frac{1}{2}}}{k_{47}(k_{27}P_{H_2} - 4k_{28}P_{C_5H_{12}})^{\frac{1}{2}}} P_{C_5H_{12}}(*) \qquad (53)$$

$$(CH_2^*) = \left\{ \frac{5k_{28}k_{-27}^{\frac{1}{2}}}{k_{46}(k_{27}P_{H_2} - 4k_{28}P_{C_5H_{12}})^{\frac{1}{2}}} + \frac{5k_{28}k_{-27}k_{-46}}{k_{46}k_{47}(k_{27}P_{H_2} - 4k_{28}P_{C_5H_{12}})} \right\} P_{C_5H_{12}}(*) \qquad (54)$$

$$(CH^*) = \left\{ \frac{5k_{28}k_{-27}^{\frac{1}{2}}}{k_{46}(k_{27}P_{H_2} - 4k_{28}P_{C_5H_{12}})^{\frac{1}{2}}} + \right.$$

$$\frac{5k_{28}k_{-27}k_{-45}}{k_{45}k_{46}(k_{27}P_{H_2} - 4k_{28}P_{C_5H_{12}})} +$$

$$\left. \frac{5k_{28}k_{-27}^{3/2}k_{-45}k_{-46}}{k_{45}k_{46}k_{47}(k_{27}P_{H_2} - 4k_{28}P_{C_5H_{12}})^{3/2}} \right\} P_{C_5H_{12}}(*) \qquad (55)$$

$$(C^*) = \left\{ \frac{5k_{28}k_{-27}^{\frac{1}{2}}}{k_{44}(k_{27}P_{H_2} - 4k_{28}P_{C_5H_{12}})^{\frac{1}{2}}} + \right.$$

$$\frac{5k_{28}k_{-27}k_{-44}}{k_{44}k_{45}(k_{27}P_{H_2} - 4k_{28}P_{C_5H_{12}})} +$$

$$\frac{5k_{28}k_{-27}^{3/2}k_{-44}k_{-45}}{k_{44}k_{45}k_{46}(k_{27}P_{H_2} - 4k_{28}P_{C_5H_{12}})^{3/2}} + \qquad (56)$$

$$\left. \frac{5k_{28}k_{-27}^{2}k_{-44}k_{-45}k_{-46}}{k_{44}k_{45}k_{46}k_{47}(k_{27}P_{H_2} - 4k_{28}P_{C_5H_{12}})^{2}} \right\} P_{C_5H_{12}}(*)$$

The sum of the fractional surface coverages of all adsorbed species and the free sites is one as shown in the expression below.

$$1 = (*) + (C^*) + (CH^*) + (CH_2^*) + (CH_3^*) + (H^*) + (\text{ADS. H.C.}) \qquad (57)$$

The coverage of all of these species has already been derived in terms of the desired variables except for (ADS. H.C.) which represents all of the hydrocarbon intermediates involved in the steps shown in equations (29)-(42). The steady flow equations relating these intermediates are

$$\begin{aligned} k_{28}P_{C_5H_{12}}(*)^2 &= k_{29}(C_5H_{11}*)(*) \\ &= k_{30}(C_5H_{10}*)(*) \\ &= k_{31}(C_5H_9*)(*) \\ &= k_{32}(C_5H_8*)(*) \\ &\vdots \\ &\text{etc.} \end{aligned} \tag{58}$$

The following expression will then express the surface coverage of the intermediates where n is the step in which the intermediate, C_xH_y*, is a reactant

$$(C_xH_y*) = \frac{k_{28}}{k_n} P_{C_5H_{12}}(*) \tag{59}$$

The surface coverage of all of these intermediates, (ADS. H.C.) is then

$$(\text{ADS. H.C.}) = \sum_{n=29}^{43} \frac{k_{28}}{k_n} P_{C_5H_{12}}(*) \tag{60}$$

It is now possible to write equation (57) in terms of only (*), $P_{C_5H_{12}}$, P_{H_2}, and constants, solve for (*) and substi-

tute the result into the rate expression, equation (49). The rate equation resulting from the mechanism shown in equations (27)-(47) is

$$\text{Rate} = k_{28}P_{C_5H_{12}}\Big\{1 + \frac{(k_{27}P_{H_2} - 4k_{28}P_{C_5H_{12}})^{\frac{1}{2}}}{k_{-27}^{\frac{1}{2}}} + \Big[\sum_{n=29}^{43}\frac{k_{28}}{k_n} + \frac{5k_{28}k_{-27}^{\frac{1}{2}}}{(k_{27}P_{H_2} - 4k_{28}P_{C_5H_{12}})^{\frac{1}{2}}}\Big(\frac{1}{k_{44}} + \frac{1}{k_{45}} + \frac{1}{k_{46}} + \frac{1}{k_{47}}\Big) + \frac{5k_{28}k_{-27}}{(k_{27}P_{H_2} - 4k_{28}P_{C_5H_{12}})} \cdot \Big(\frac{k_{-44}}{k_{44}k_{45}} + \frac{k_{-45}}{k_{45}k_{46}} + \frac{k_{-46}}{k_{46}k_{47}}\Big) + \frac{5k_{28}k_{-27}^{3/2}}{(k_{27}P_{H_2} - 4k_{28}P_{C_5H_{12}})^{3/2}}\Big(\frac{k_{-44}k_{-45}}{k_{44}k_{45}k_{46}} + \frac{k_{-45}k_{-46}}{k_{45}k_{46}k_{47}}\Big) + \frac{5k_{28}k_{-27}^2}{(k_{27}P_{H_2} - 4k_{28}P_{C_5H_{12}})^2}\,\frac{k_{-44}k_{-45}k_{-46}}{k_{44}k_{45}k_{46}k_{47}}\Big]P_{C_5H_{12}}\Big\}^{-2} \quad (61)$$

This can be rewritten as

$$\text{Rate} = \frac{C}{4}P_{C_5H_{12}}\Big\{1 + A(BP_{H_2} - CP_{C_5H_{12}})^{\frac{1}{2}} + \Big[D + E(BP_{H_2} - CP_{C_5H_{12}})^{-\frac{1}{2}} + F(BP_{H_2} - CP_{C_5H_{12}})^{-1} + G(BP_{H_2} - CP_{C_5H_{12}})^{-3/2} + H(BP_{H_2} - CP_{C_5H_{12}})^{-2}\Big]P_{C_5H_{12}}\Big\}^{-2} \quad (62)$$

The meaning of the constants in equation (62) is obvious when compared to equation (61).

The rate expression was then fit to the experimental data by varying the constants A - H . Table V shows the optimum values for the constants when fit to data taken at 468K along with the units for each.

Table V. Values for the rate constants in the rate law (equation (62)) at 468K.

Const.	Value	Units
A	0.01	$molec.^{-\frac{1}{2}}\text{-}site^{\frac{1}{2}}\text{-}sec.^{\frac{1}{2}}$
B	0.195	$molec.\text{-}site^{-1}\text{-}sec.^{-1}(10^{-3}\ torr)^{-1}$
C	0.0012	$molec.\text{-}site^{-1}\text{-}sec.^{-1}(10^{-3}\ torr)^{-1}$
D	5.4×10^{-5}	$(10^{-3}\ torr)^{-1}$
E	9.1×10^{-3}	$molec.^{\frac{1}{2}}\text{-}site^{-\frac{1}{2}}\text{-}sec.^{-\frac{1}{2}}(10^{-3}\ torr)^{-1}$
F	0.485	$molec.\text{-}site^{-1}\text{-}sec.^{-1}(10^{-3}\ torr)^{-1}$
G	0	$molec.^{3/2}\text{-}site^{-3/2}\text{-}sec.^{-3/2}(10^{-3}\ torr)^{-1}$
H	0	$molec.^{2}\text{-}site^{-2}\text{-}sec.^{-2}(10^{-3}\ torr)^{-1}$

The surface concentrations of the adsorbed hydrocarbon intermediates involving more than one carbon atom is expected to be very small while the concentrations of the single carbon atom species will build up on the surface along with hydrogen adatoms and slowly react to form methane. Thus the exact steps involved in the dissociation

of neopentane into one carbon atom fragments are not very important and will have little if any effect on the fit of the model with the experimental data. The concentrations of the surface species will vary under different reaction conditions and will be reflected in the values (zero or non-zero) of constants E - H; however, there is no one to one correspondence between a particular species and a particular constant. The excellent fit of the data with the model when G = H = 0 implies that the surface is populated by CH_3 and CH_2 species but not by a significant amount of C or CH species. The minimum necessary condition for these constants to be zero in $k_{-45} = 0$.

The hydrogen order kinetic data shown in Figure 12 were obtained at 468K and a neopentane pressure of 32×10^{-3} torr on four different days on one film. The scatter (±15%) is greatest at the center of the hydrogen pressure range covered where there is an abundance of data points. The theoretical fit to the data appears to be quite good. Figures 13 and 14 are hydrogen order plots obtained at lower neopentane pressures, (13 and 14) $\times 10^{-3}$ torr, respectively. The data in Figure 14 were obtained on two different days over different films with overlap of data at $\log P_{H_2} = 1.0$ to 2.8. The agreement of data in the range of overlap is excellent as is the fit with the model. The data at the low pressure end of the hydrogen pressure exhibit a slope of

Figure 12. Hydrogen order results collected on four different days. The results predicted by the model are indicated by the solid line.

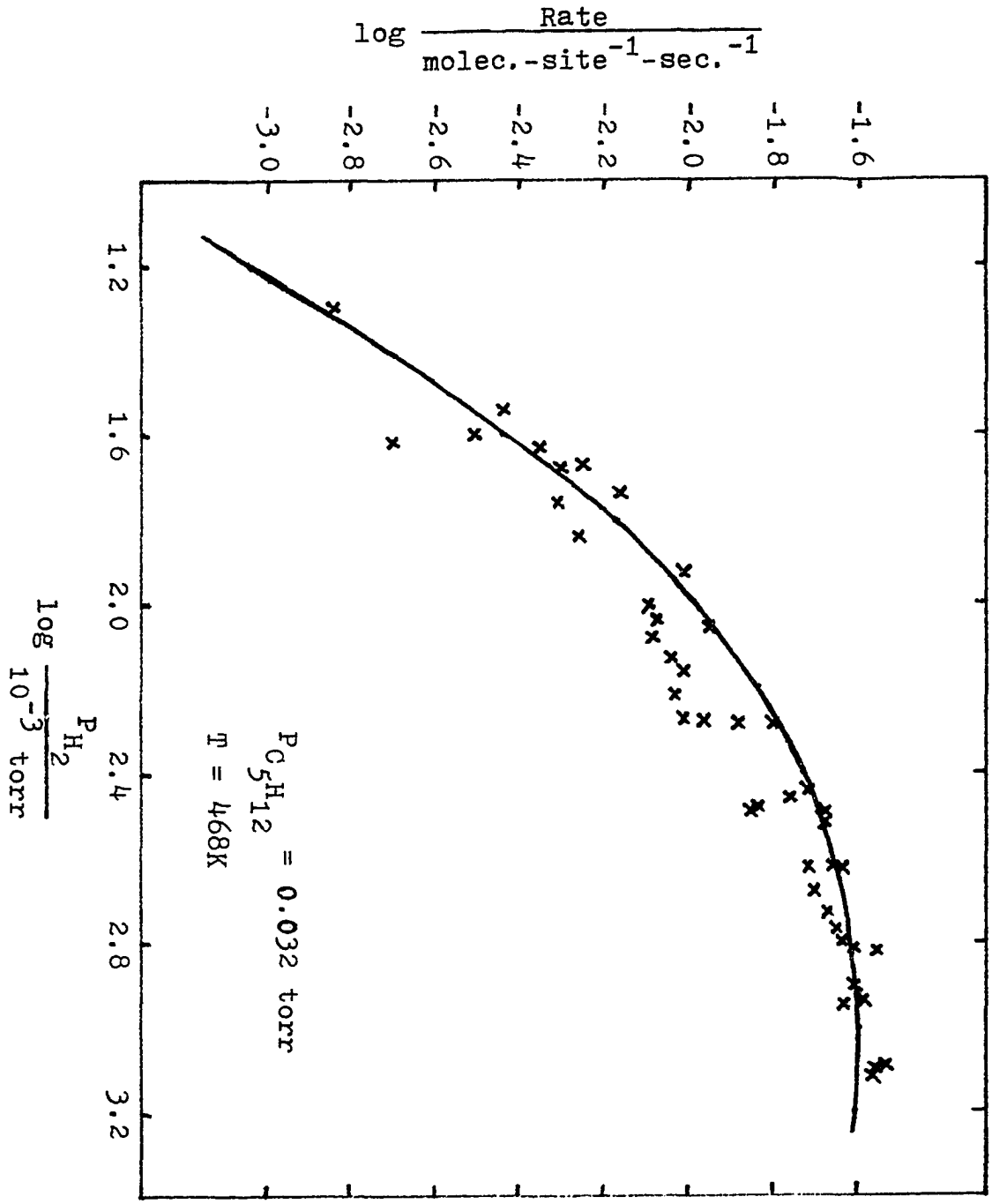
log Rate / molec.-site^{-1}-sec.$^{-1}$
-1.6
-1.8
-2.0
-2.2
-2.4
-2.6
-2.8
-3.0
1.2
1.6
2.0
2.4
2.8
3.2
log P_{H_2} / 10^{-3} torr
$P_{C_5H_{12}}$ = 0.032 torr
T = 468K

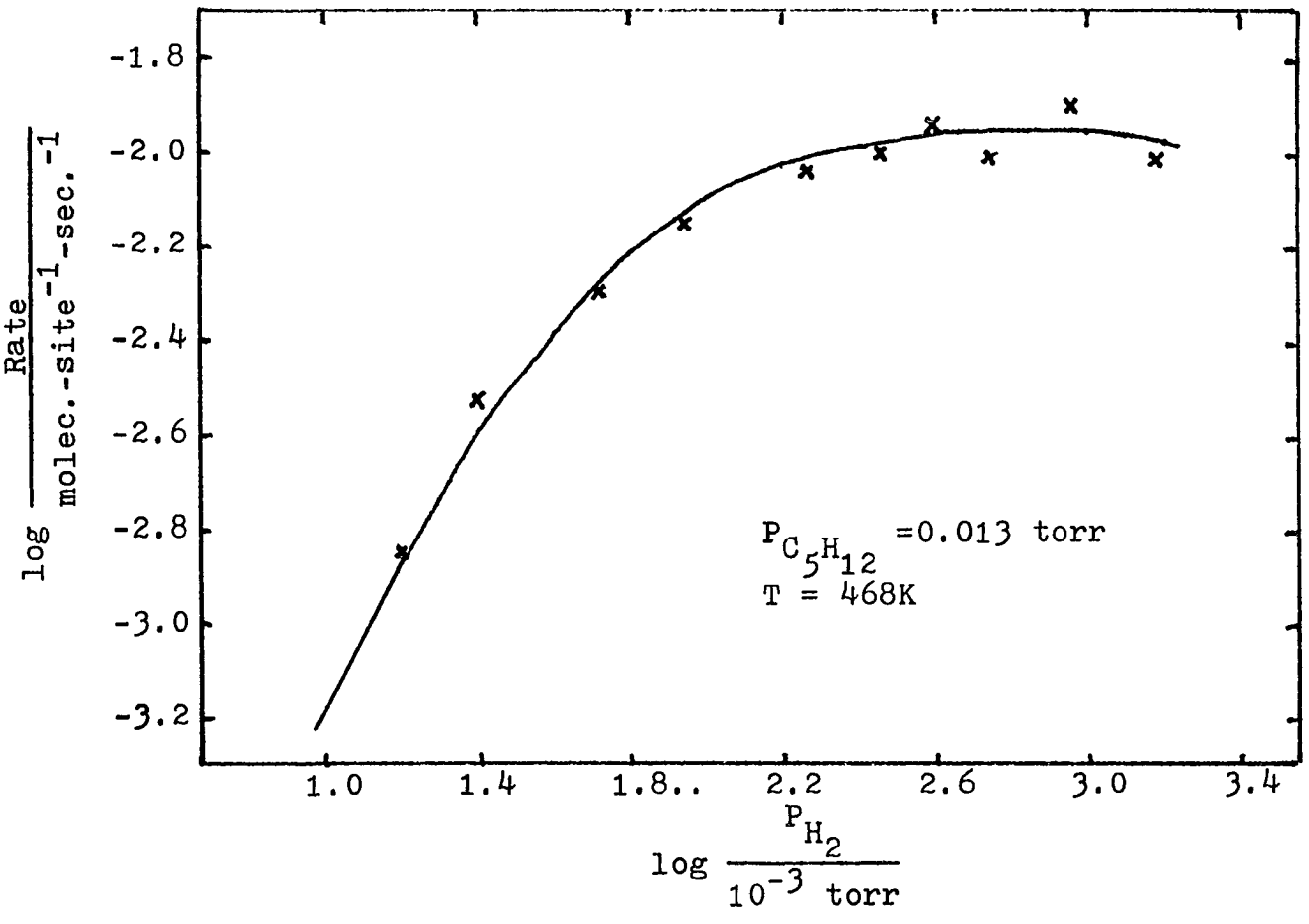

Figure 13. The fit of the model to a hydrogen order plot at $P_{C_5H_{12}}$ = 0.013 torr.

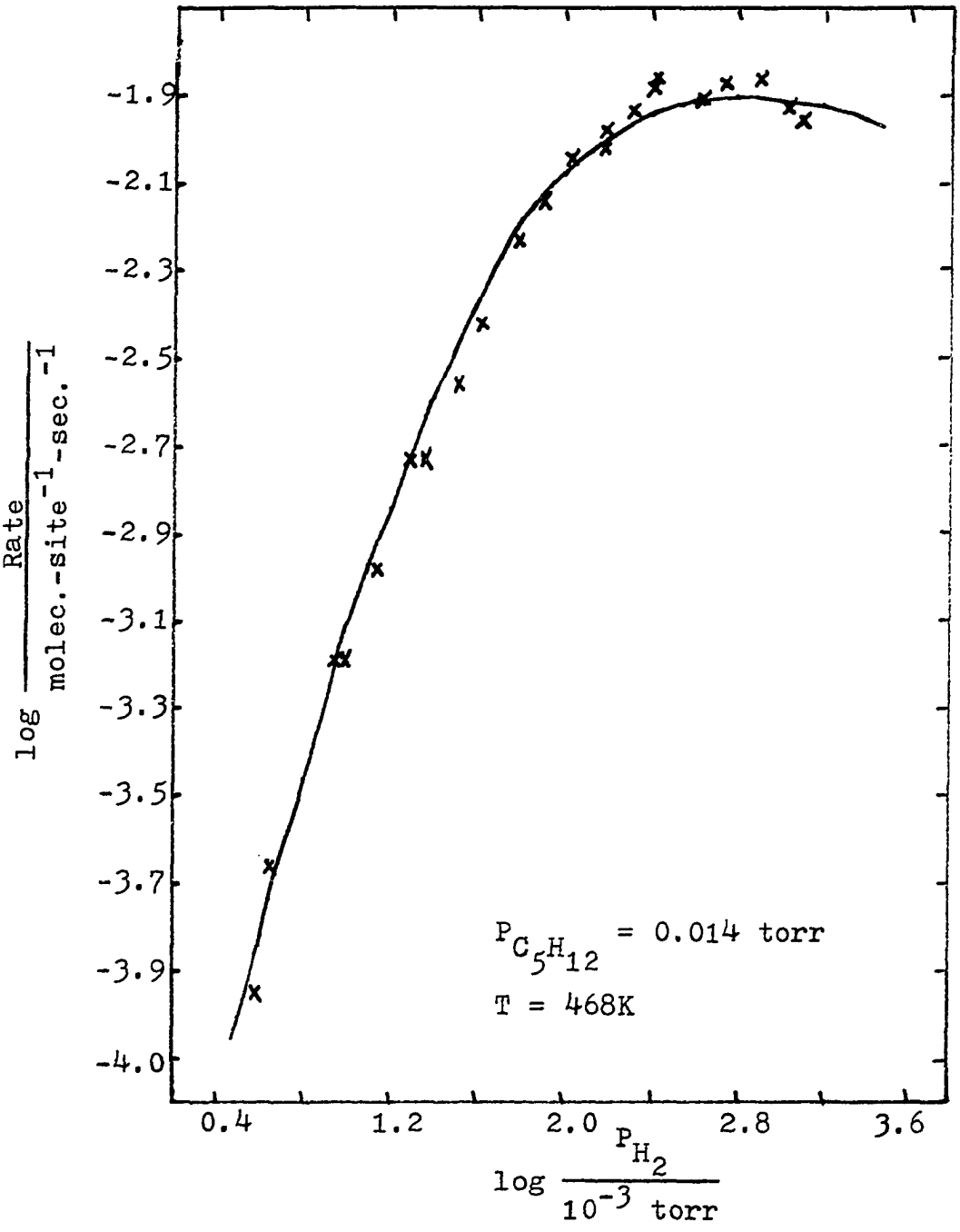

Figure 14. The fit of the model to a hydrogen order plot at $P_{C_5H_{12}}$ = 0.014 torr.

+2.0 which was the most positive order with respect to the hydrogen partial pressure obtained. The data shown in Figure 13 were collected in one day over a slightly smaller pressure range than was used in Figure 14; again the fit to the theory is very good. Figures 15-17 show the theoretical fit to neopentane order plots where the hydrogen pressures used were 28 x 10^{-3}, 270 x 10^{-3} and 1.00 torr, respectively. The maximum positive order was +0.95 at low neopentane pressures in Figure 17 and -0.8 at high neopentane pressures in Figure 16. The maximum in Figure 16 appears to occur at higher neopentane pressures than the model predicts; however, the difference in the maxima could easily be due to scatter in the experimental data.

The model predicts zero order with respect to the partial pressure of methane as shown in Figure 18. These data were obtained at P_{H_2}=0.110 torr, $P_{C_5H_{12}}$=7 x10^{-3} torr, T=468K and methane pressures in the range (0.32 - 25) x 10^{-3} torr; the log rate versus log P_{CH_4} plot has a slope (indicated by the dashed line) of -0.03 in close agreement with the zero slope implied by the model.

The theoretical rate expression given by equation (62) using the constants in Table V agrees with most of the experimental data as summarized below. It

a) Predicts methane as the only product since neopentane dissociates into single carbon fragments upon adsorp-

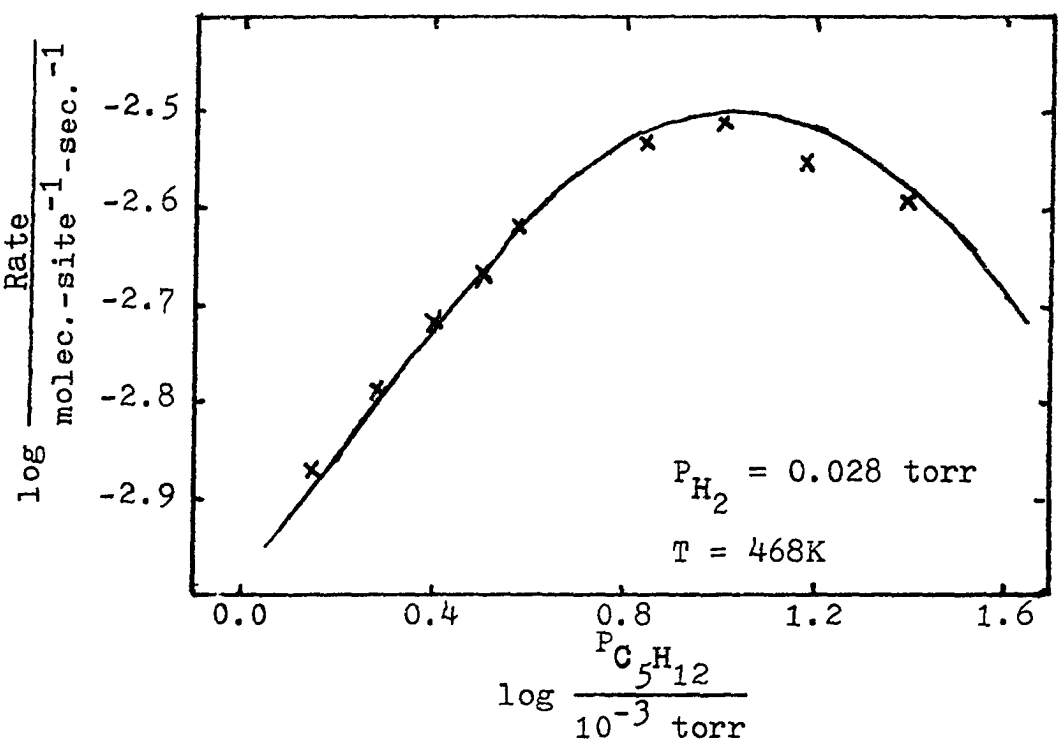

Figure 15. The fit of the model to the neopentane order results obtained at P_{H_2} = 0.028 torr.

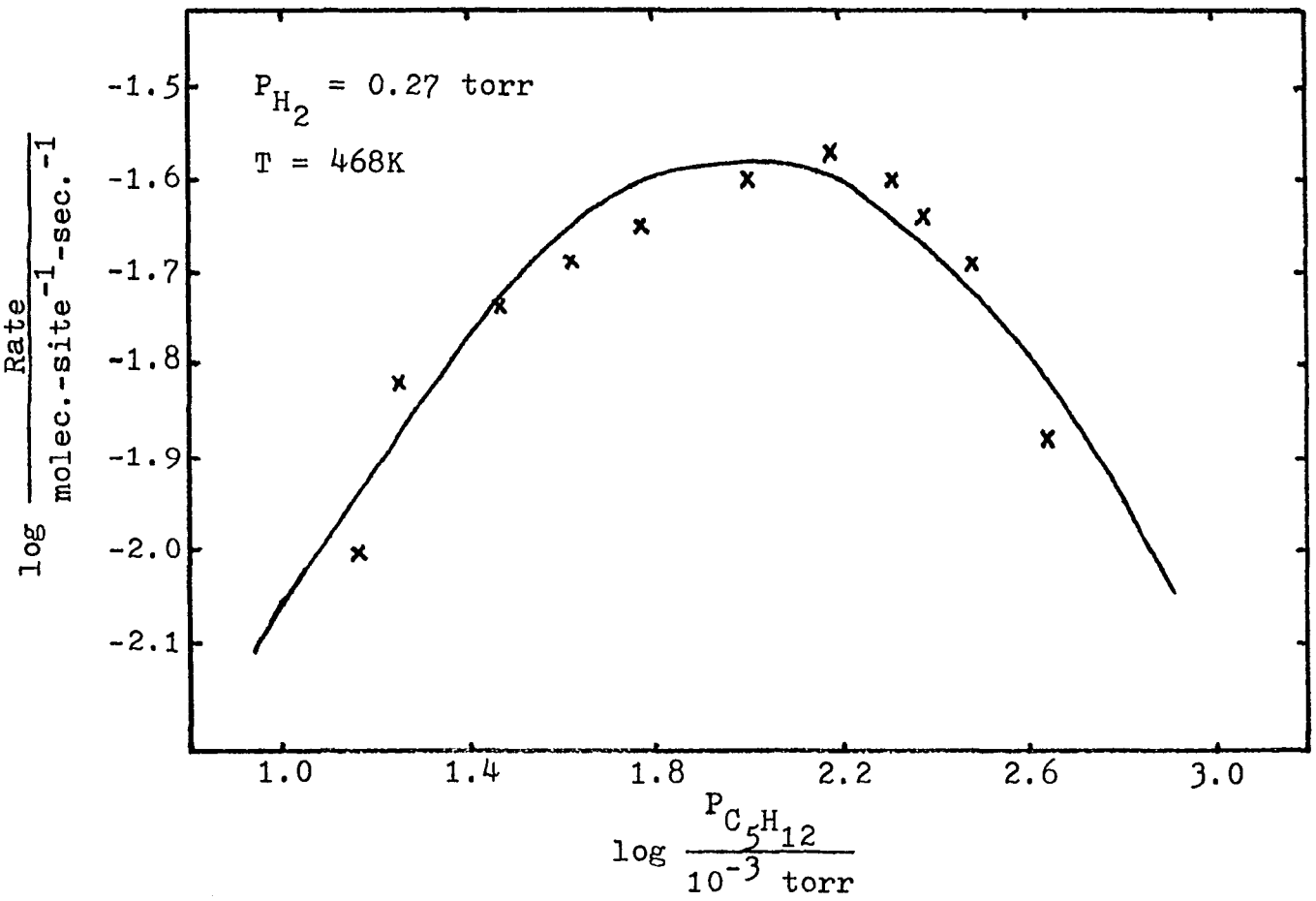

Figure 16. The fit of the model to neopentane kinetic order results obtained at P_{H_2} = 0.27 torr.

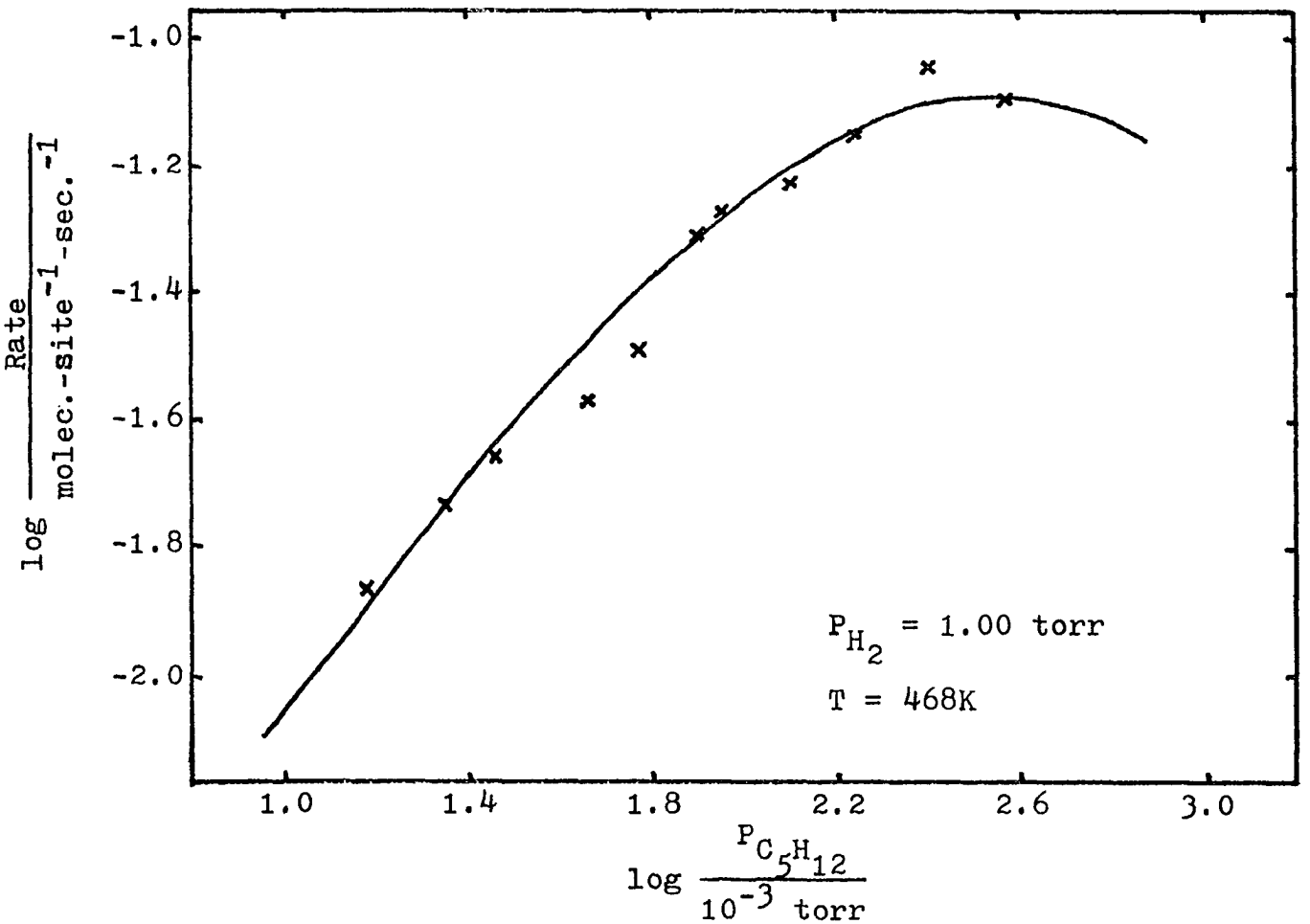

Figure 17. The fit of the model to a neopentane order plot at P_{H_2} = 1.00 torr.

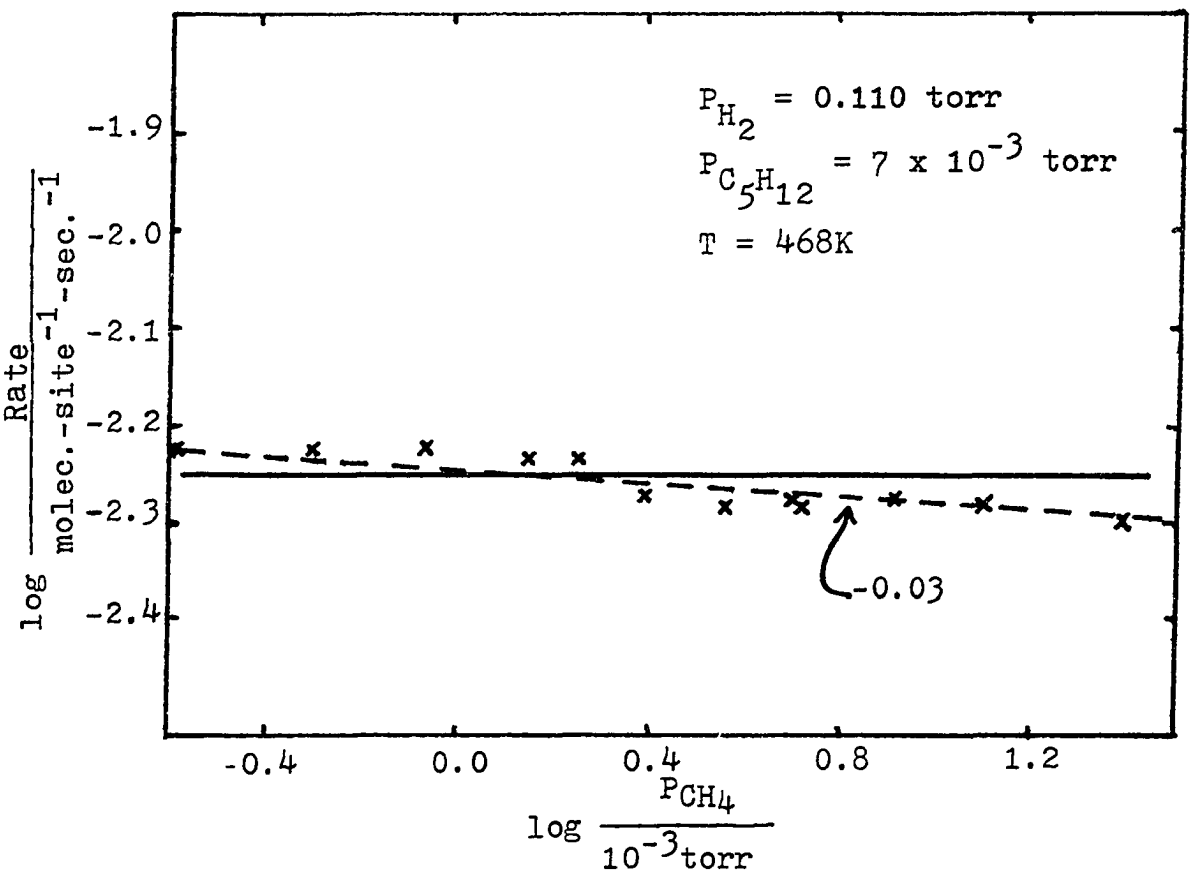

Figure 18. The variation in the rate of the hydrogenolysis of neopentane with methane pressure. The solid line is the zero order predicted by the model and the dashed line is the best fit to the data and has a slope of -0.03.

tion

b) Predicts neopentane exchange will not occur for the same reason as in a) if there is only one type of adsorbed neopentane species.

c) Gives good fits to all of the kinetic order experimental data collected for neopentane and methane and all of the data collected for hydrogen orders except those obtained at very low and high neopentane pressures (to be discussed shortly).

d) Agrees with flash desorption experimental results which indicate that neopentane adsorption does not result in the formation of intermediate hydrocarbons (i.e. containing more than one carbon atom) on the surface.

The theory appears to fall short (at least the modifications implied by ignoring the surface concentrations of C* and CH*) when compared to the experimental results of the neopentane adsorption experiments which indicated that when neopentane alone was adsorbed on the surface, the surface species formed consisted of CH or bare carbon atoms and hydrogen (most of which desorbs in the absence of gas phase hydrogen). It must be realized that there are two major differences between the conditions at which the neopentane adsorption studies and the kinetic studies were conducted; the adsorption studies utilized very low neopentane pressure and no hydrogen, whereas the kinetic studies in general used

higher neopentane pressures and significant amounts of hydrogen. Several experiments were conducted at very low neopentane pressures ~1 x 10^{-3}torr; an example is shown in Figure 19 along with the theoretical fit using the values for the constants shown in Table V (dashed curve). It should be noted that the pressure of neopentane is changing, as indicated at the top of the figure, as the hydrogen pressure is increased, as indicated at the bottom of the figure, even though the same amount of neopentane was dosed into the cell at the beginning of each experiment (this has been discussed previously). The fit in Figure 19 is quite obviously not very good. The poor fit and the discrepancy between the extent of dehydrogenation of adsorbed hydrocarbon species experimentally determined and that used in the theoretical fit can be explained as follows: at very low neopentane pressures the surface is very likely populated with highly dehydrogenated species; however, as the pressure of neopentane is increased, the adsorbed intermediates are unable to dehydrogenate as fully and so the surface tends to be populated with CH_2 species instead of CH or bare carbon. The solid curve in Figure 19 is the theoretical fit of the rate expression shown in equation (62) using the same constants as shown in Table V except that C = 0.006 molec.-site^{-1}-sec.$^{-1}$ (10^{-3} torr)$^{-1}$ and G = 0.73 molec.$^{3/2}$-site$^{-3/2}$-sec.$^{-3/2}$(10^{-3} torr)$^{-1}$. The necessity for including the term involving the

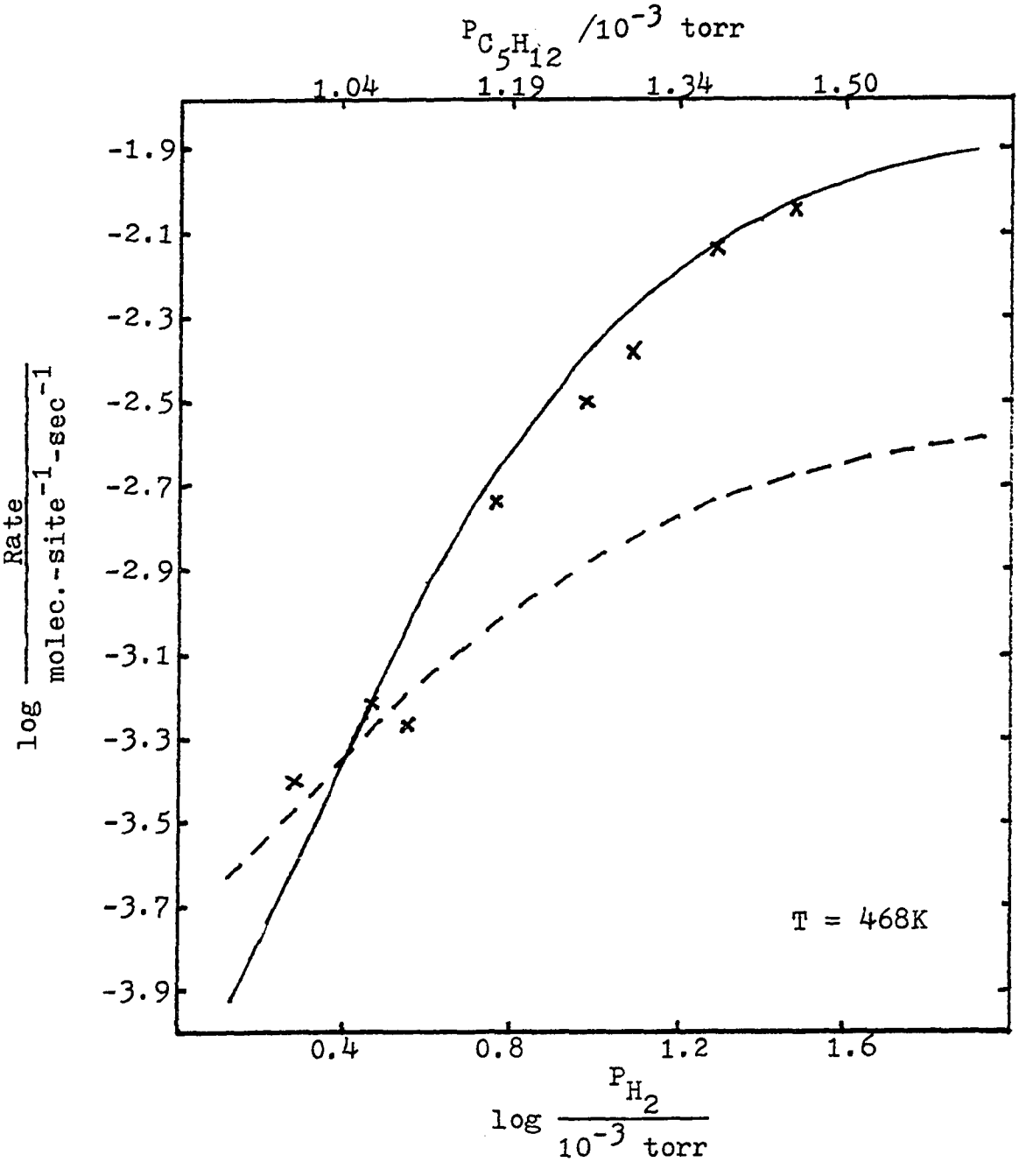

Figure 19. The fit of results obtained at very low neopentane pressures (see top of figure) and various hydrogen pressures (indicated at bottom of figure). The dashed curve is the fit to the original model and the solid curve is the fit to the modified one.

constant G implies that the predominant adsorbed species is CH in this case and not CH_2. The constant C is simply k_{28}, the rate constant for the adsorption of neopentane, and its increase indicates one of two things. Either the neopentane is able to adsorb on the surface more easily at low neopentane pressures, or the ability for neopentane to adsorb is enhanced on the films deposited at room temperature and later sintered. (All of the low neopentane data were obtained on films deposited at room temperature.) The room temperature films have a much higher active surface area than the other films and perhaps the increase in k_{28} reflects the increased probability that a neopentane molecule will strike an active surface site rather than an inactive one. The main effect of varying the constant C is to shift the position of the curve along the y-axis. The position of the experimental curve along the y-axis depends on the amount of active surface sites as determined by the desorption of methane during hydrogen flushes. That method for determining the number of active sites gave results which were within 10% of each other on films with a large number of active surface but the data for films with low active surface areas often varied by a factor of two. In some cases the active surface sites were determined by averaging the results for a film instead of using the actual value determined on a particular day. Thus, errors in determining the number of active surface

sites would be masked by choosing an appropriate value for C.

Figures 20 and 21 are similar to the previous figure and show the reasonable fit to the rate expression derived from a mechanism which assumes the presence of a highly dehydrogenated intermediate adsorbed on the surface. The data in Figure 21 show the poorest fit to the theory, but even so the maximum deviation is only 15%.

The data obtained at high neopentane pressures are also not well fit by the theory as is shown by Figure 22 where the dashed line is the theoretical fit to equation (62) using the constants in Table V. The fit is vastly improved when F is reduced to 0.242 molec.-site^{-1}-sec.$^{-1}$(10^{-3} torr)$^{-1}$ and C to 0.009 molec.-site^{-1}-sec.$^{-1}$(10^{-3} torr)$^{-1}$ as shown by the solid line. The decrease in F is indicative of a reduction in the amount of surface CH_2 as compared to the amount present at lower neopentane pressures and thus the surface composition (H/C) will be higher. Thus, although the theoretical fit to the experimental data collected for neopentane. orders is very good, the fit to the hydrogen order data is good for neopentane pressures in the range (14 to 32) x 10^{-3} torr but modifications of the theory are necessary for data collected at higher or lower neopentane pressures. This will be discussed in more detail later.

Comparison of equation (62) with equation (61) reveals that values for some of the rate constants can be determined

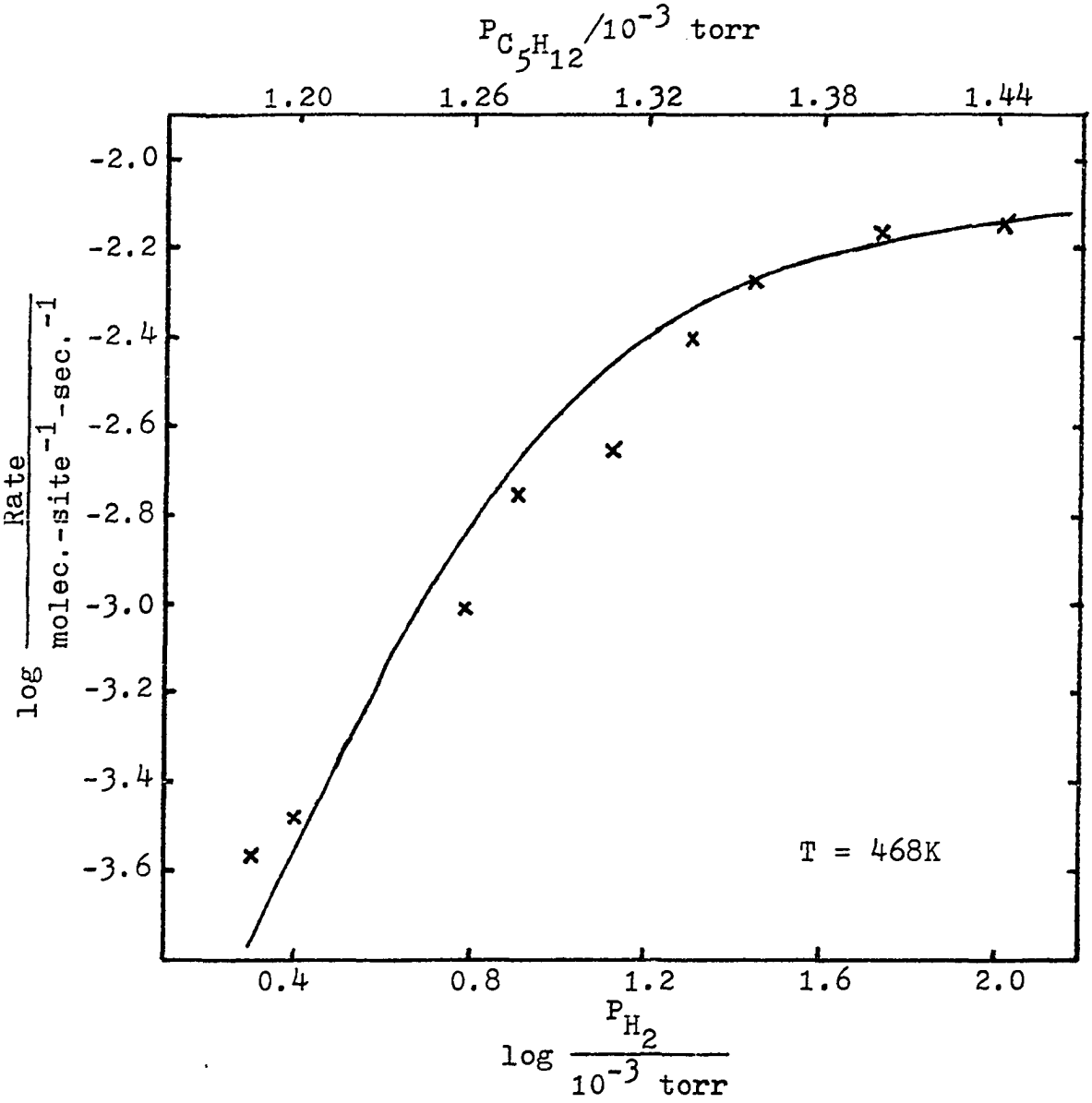

Figure 20. The fit of low neopentane pressure results with the modified theory.

Figure 21. The fit of low neopentane pressure kinetic data with the modified model.

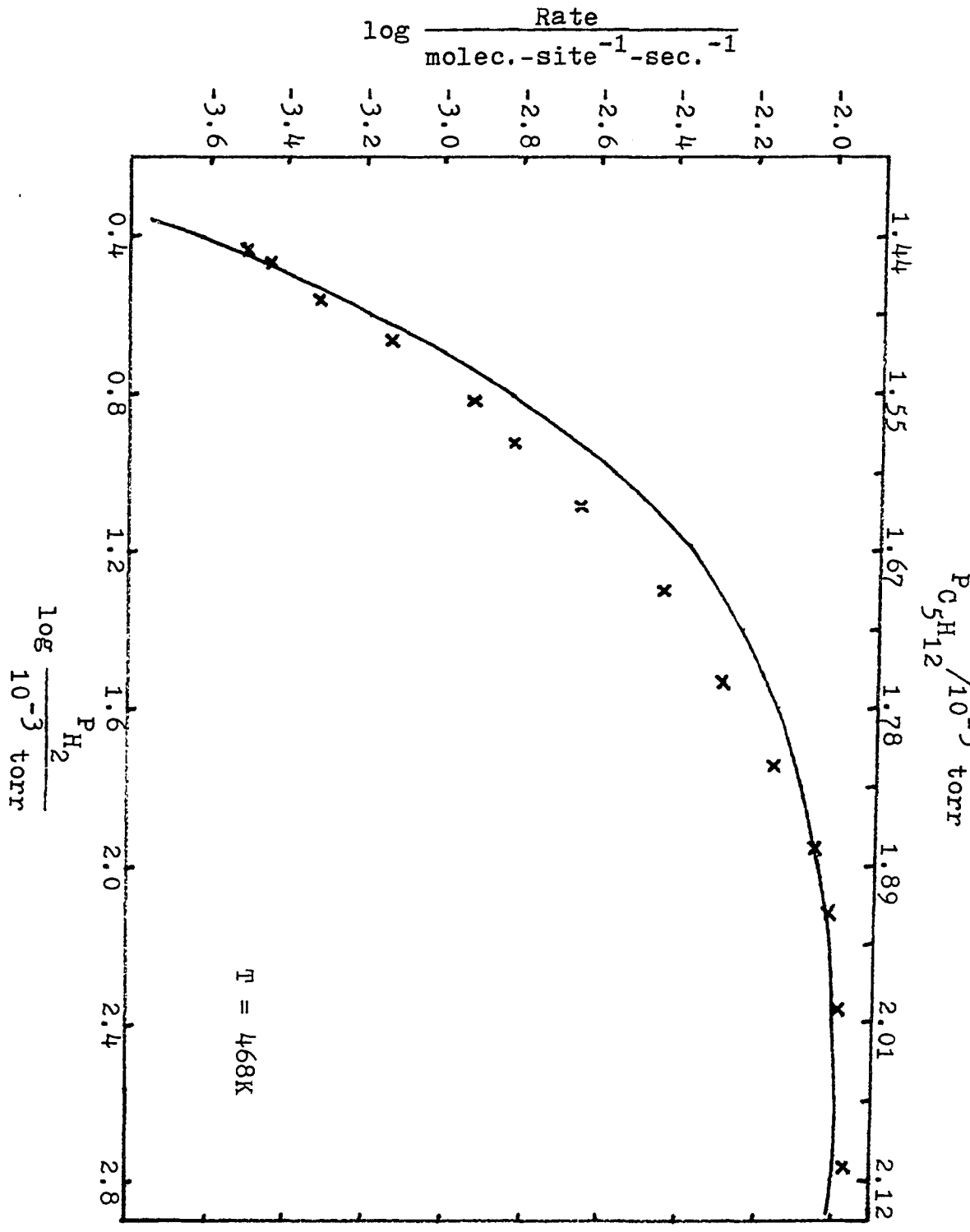
log Rate / molec.-site^{-1}-sec.$^{-1}$
-2.0
-2.2
-2.4
-2.6
-2.8
-3.0
-3.2
-3.4
-3.6
1.44
1.55
1.67
1.78
1.89
2.01
2.12
$P_{C_5H_{12}}/10^{-3}$ torr
0.4
0.8
1.2
1.6
2.0
2.4
2.8
log P_{H_2} / 10^{-3} torr
T = 468K

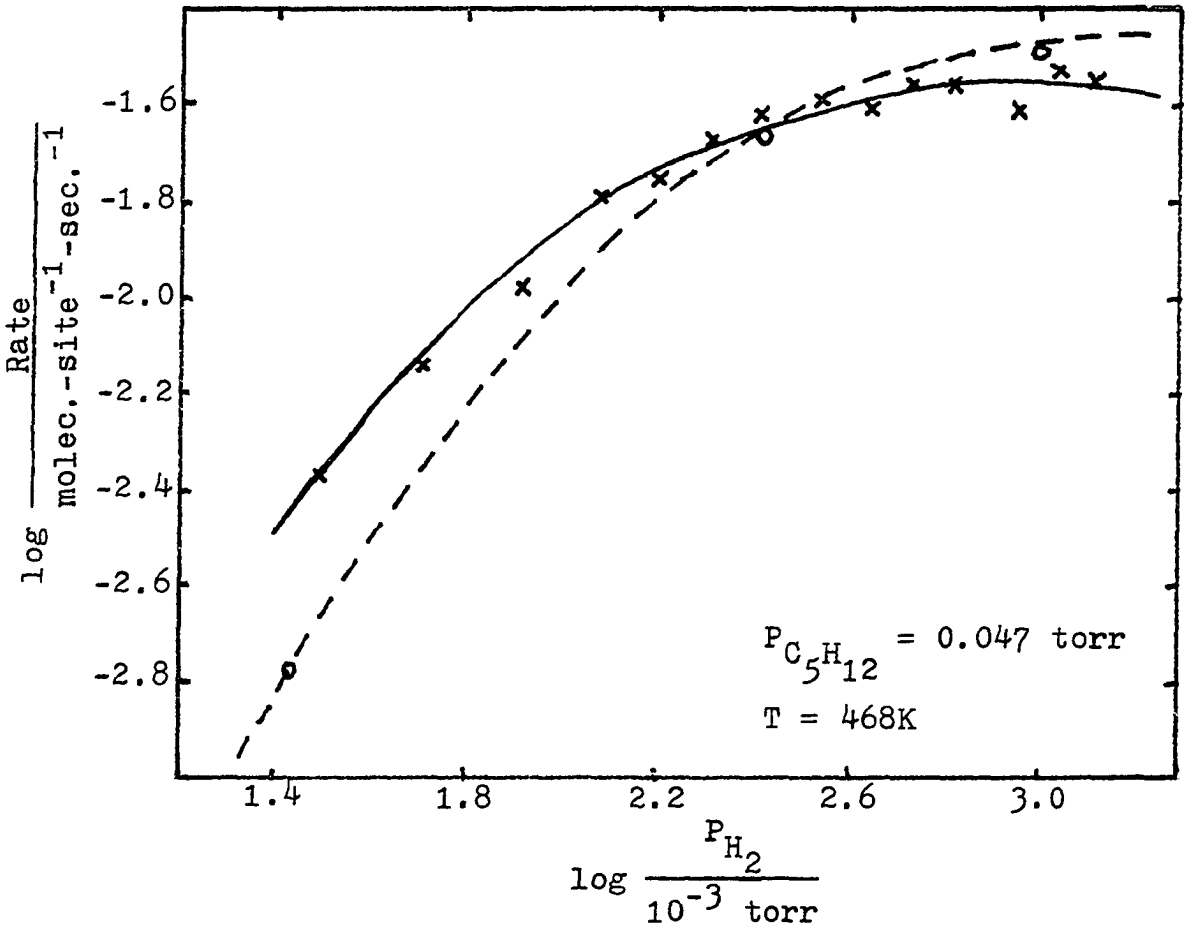

Figure 22. The hydrogen order results obtained at high neopentane pressure fit to the original theory (dashed line) and to the modified version (solid line). The o's are data taken from Figures 15-17 at 0.047 torr neopentane.

from the constants A - G and more importantly so can the equilibrium constant for the adsorption of hydrogen in equation (27); $K_{27} = A^2B = 1.95 \times 10^{-5}(10^{-3}\text{torr})^{-1} = 1.95 \times 10^{-2}$ torr^{-1} at 468K. It is often difficult to discuss values obtained for rate and equilibrium constants because so few have been reported in the literature. There have however been determinations (obtained by curve fitting procedures similar to those used here) of the equilibrium constant for hydrogen adsorption on iridium thin films by Mahaffy and Hansen (27) and on ruthenium thin films by Slaughter (57). The equilibrium constant was reported to be 2.5×10^3 torr^{-1} and 20 torr^{-1} at 373K and 473K respectively on iridium and on ruthenium it was reported to be 1×10^{-3} torr at 573K. The result obtained here of 1.95×10^{-2} torr^{-1} at 468K appears to be quite reasonable in light of these other results. Hydrogen has been reported to flash off iridium at 423K (37,38,52) and consequently it would appear that the equilibrium constant should be small at this temperature. Differences between the results of Mahaffy and Hansen and this work may be due to differences in the reactivity of the films caused by slightly different deposition techniques.

The ratio of the square root of the hydrogen adsorption equilibrium constant to the methane adsorption equilibrium constant was found in a previous section to be 0.0302 $\text{torr}^{\frac{1}{2}}$ which when used with the hydrogen adsorption equilibrium

constant reported above yields a methane adsorption constant of 4.63 $torr^{-1}$. Frennet (58) determined the equilibrium constant for methane adsorption on rhodium films as indicated by the equation:

$$CH_4 + H^* \underset{}{\overset{K_{63}}{\rightleftharpoons}} CH^* + 2H_2 \qquad (63)$$

This is somewhat different from equation (1) which was assumed as the reaction involved in methane adsorption, however the equilibrium constants can be compared keeping this difference in mind. Frennet found $K_{63} = 6.6 \times 10^{-3}$ torr at 423K and 0.12 torr at 498K. The result $K_1 = 4.62$ $torr^{-1}$ determined here is not outrageous especially considering the differences in the reaction equations for the adsorption of methane. The values for k_{28}, k_{27} and k_{-27} can be found directly from the constants A, B, and C; independent literature values are not available for comparison. It should also be realized that the constants are determined so as to fit the experimental data and so to correlate the absolute values with physical quantities is somewhat questionable.

The results of the theoretical fit of equation (62) to the experimentally determined kinetic orders are summarized below.

1) All of the neopentane kinetic order data are fit very well (Figures 15-17).

2) The hydrogen kinetic order data:

a) fits very well at constant neopentane pressures in the range (14-32) x 10^{-3} torr (Figures 12-14).

b) fits poorly outside of the range mentioned in a).

Thus, although the model in which the neopentane surface intermediate is predominately CH_2 fits the majority of the kinetic data, there are certain conditions at which the theory proposed does not explain the results. The change in the value of C used to fit the low neopentane pressure data cannot be applied to the high pressure results because these results were obtained on the same film as the rest of the kinetic data. In addition, if the rates of the reaction (o's) at 47 x 10^{-3} torr obtained from Figures 15-17 for P_{H_2} = (28, 270 and 1000) x 10^{-3} torr respectively are plotted with the other results (x's) at this neopentane pressure, it is obvious from Figure 22 that the theory (dashed line) fits the data indicated by o's although the fit to the x's is poor. Thus the fit to three data points collected on different days agrees with the theoretical plot while the data collected on one day does not seem to. A closer inspection of the hydrogen order results reveals that although the discrepancy between the experimental and theoretical rates at low hydrogen pressures is large, an increase of about 10% in the hydrogen pressures dosed into the cell would allow the experimental data to fit the theoretical. A 10% error in pres-

sure measurement is greater than normally expected, but not impossible.

The neopentane pressures used in the neopentane order kinetic runs did not include pressures as low as 1×10^{-3} torr so the check used above cannot be applied to the hydrogen order data at very low neopentane pressure. In this case, however, the same data were reproduced on several occasions and thus the poor fit is very likely real.

It is quite likely that the degree of dissociation at low neopentane pressures is higher than at high neopentane pressures. The H/C ratio of the hydrocarbon fragments on the surface is probably gradually increasing from ~ 1 at very low ($<2 \times 10^{-3}$ torr) neopentane pressures to ~ 2 at higher ($>10 \times 10^{-3}$ torr) pressures. The upper limit of 10×10^{-3} torr is the pressure at which the maximum amount of carbon is left on the surface after evacuation; thus, if varying neopentane pressures are dosed into the reaction cell and a plot of the pressure of methane desorbed (during a hydrogen flush) versus neopentane pressure is made, the resulting curve will increase sharply for the first five millitorr and then start to level off and will have a constant value for pressures greater than 10 millitorr. This clearly reflects the amount of chemisorbed carbon and it is suggested that it may also reflect the H/C ratio on the surface. At pressures greater than 10 millitorr the surface coverage

is at its highest and the H/C ratio of the hydrocarbon fragments will be the same because the surface sites are occupied by the fragments and the free surface sites required to reduce the H/C ratio of the adsorbed species are unavailable. At lower pressures, however, some of the surface sites are vacant and thus further dissociation of the fragments can take place. The above discussion dealt with the case when only neopentane was present and must be extended to include the case when hydrogen is dosed with the neopentane. In order for the discussion above to apply when hydrogen is also present, the carbon fragments must be adsorbing on sites different from the sites at which hydrogen is adsorbing or the carbon fragments must be able to displace the hydrogen so that the degree of dissociation is due solely to the neopentane partial pressure. The first hypothesis excluding competitive adsorption can be discarded because of the excellent agreement between the theory, which assumes competition between hydrogen and hydrocarbon for the same sites, and the majority of the data. The second hypothesis appears to be reasonable because at these temperatures hydrogen is very weakly bound to the surface and will move around on it while the carbon is more strongly chemisorbed. Thus, although one might think that at high hydrogen pressures the extent of dissociation of hydrocarbon fragments on the surface would be less than at low hydrogen pressures, the

data suggest that the extent of dehydrogenation is instead dependent mainly on the hydrocarbon pressure. This effect has not been seen in the past because extremely few studies have been conducted with hydrocarbon pressures less than 10×10^{-3} torr.

Hydrogenolysis experiments in the present study resulted in the production of only one product - methane - while other studies resulted in the production of several hydrocarbons. One very major difference is the pressure range at which the reaction was studied, the other studies having been done at pressures greater than 1 torr. This difference seems very important in light of the different results obtained at neopentane pressures of 1×10^{-3} torr and at greater than 10×10^{-3} torr. It seems plausible that the high neopentane pressures used in the other studies might inhibit the fragmentation of neopentane upon adsorption so that a different mechanism would be necessary and different products could be observed. In addition, if the neopentane adsorbs <u>via</u> only carbon - hydrogen bond rupture, the exchange results obtained by various researchers as previously discussed can be explained.

The difference in the amount of active surface sites on films deposited at room temperature and at the sintering temperature is striking. The increase in active surface sites on the room temperature films suggests that the active

site may be a step or a kink site and not a group of terrace atoms since it is expected that these films contain more surface imperfections than the other films. The population of the active sites is much less than the number of atoms (1×10^{15} /cm^2) which one would find in a (100) oriented film deposited in the same reaction cell. If it was assumed that there are 1×10^{15} atoms/cm^2 and that each surface site determined by the methane production during a hydrogen flush consists of only one surface atom, the surface areas of the films used would be 6 to 120 cm^2. The geometric surface area of the reaction cell is 250 cm^2 and the surface area of a film which is not generally a smooth surface is usually larger than the geometric surface area. Thus, the assumption that every surface atom is an active surface site yields surface areas which are much too small; the number of active sites is small compared to the total number of surface atoms. Possibly only steps or kinks in the surface are active. Another explanation is that the surface site is actually composed of several surface atoms. Thus, the surface site is either an iridium atom or group of atoms at a kink or step or an ensemble of atoms on a terrace but is not a single atom in a terrace.

SUMMARY AND SUGGESTIONS FOR FUTURE INVESTIGATIONS

The kinetic results, flash desorption results, isotopic exchange results and neopentane adsorption results are fit by a model in which neopentane is irreversibly adsorbed on the surface and CH_3, CH_2, CH, C and H are in competition for the active surface sites. The mechanism by which neopentane dissociates into single carbon atom fragments is not postulated because these steps are fast compared to the hydrogenation of the surface species and thus little information about the individual steps can be obtained. The model allows the surface concentrations of the hydrocarbon fragments to vary depending upon the reaction conditions; at neopentane pressures $<2 \times 10^{-3}$ torr the surface is populated predominantly by CH species while at pressures $>10 \times 10^{-3}$ torr the CH_2 species predominates. It has been postulated that the active surface sites are kink or step sites or an ensemble of iridium atoms in a terrace.

The kinetic data obtained were very well fit by the model, however the limitations of the capacitance manometer prevented determination of the presumed negative order with respect to the partial pressure of hydrogen at hydrogen pressures greater then 0.8 torr. It would be of interest to use a higher pressure capacitance manometer to determine if the actual hydrogen order is as predicted.

The surface species mentioned above were postulated on

the basis of the hydrogen to carbon ratio on the surface determined from neopentane adsorption experiments. Nuclear magnetic resonance and electron loss spectroscopy are two techniques which would allow the elucidation of the species actually present on the surface.

There are also many experiments which could be done to determine the effect of changing film deposition conditions on the number of active sites (and therefore on the overall activity of the film). The various films could be examined with an electron microscope to determine the differences in surface morphology.

It would also be interesting to determine if the product distribution is affected by the addition of small amounts of contaminants (i.e. oxygen or nitrogen) to the reaction mixture.

LITERATURE CITED

1. Cimimo, A.; Boudart, M.; Taylor, H. S. J. Phys. Chem. 1954, 58, 796.
2. Kemball, C.; Taylor, H. S. J. Amer. Chem. Soc. 1948, 70, 345.
3. Sinfelt, J. H. U. S. Patent 3,953,368, 1976.
4. Rasser, J. C. "Platinum - Iridium Reforming Catalysts" Delft Univ. Press: Delft, 1977.
5. Boudart, M.; Ptak, L. D. J. Catal. 1970, 16, 90.
6. Boudart, M.; Aldag, A. W.; Ptak, L. D.; Benson, J. E. J. Catal. 1968, 11, 35.
7. Anderson, J. R.; Avery, N. R. J. Catal. 1966, 5. 446.
8. Anderson, J. R.; Baker, B. G. Proc. R. Soc. Lond. A. 1963, 271, 402.
9. Anderson, J. R; Baker, B. G. Nature 1960, 187, 937.
10. Sárkány, A.; Guczi, L.; Tétényi, P. Acta Chim. Acad. Sci. Hung. 1978, 96, 27.
11. Foger, K.; Anderson, J. R. J. Catal. 1979, 59, 325.
12. Foger, K.; Anderson, J. R. J. Catal. 1978, 54, 318.
13. Dowie, R. S.; Kemball, C.; Kempling, J. C.; Whan, D. A. Proc. R. Soc. Lond. A. 1972, 327, 491.
14. Kemball, C.; Kempling, J. C. Proc. R. Soc. Lond. A. 1972, 329, 391.
15. Kemball, C. Trans. Faraday Soc. 1954, 50, 1344.
16. Mills, G. A.; Heinemann, H.; Milliken, T. H.; Ohland, A. G. Ind. Eng. Chem. 1953, 45, 134.
17. Kempling, J. C.; Anderson, R. B. "Proceedings of the 5th International Congress on Catalysis", North Holland, Amsterdam, 1973.
18. Yao, H. C.; Shelef, M. J. Catal. 1979, 56, 12.

19. Kuznetsov, B. N.; Yermakov, Y. I. J. Molecular Catal. 1979, 4, 49.

20. Samman, N. G. "Proceedings of the 5th International Congress on Catalysis", North Holland, Amsterdam, 1973.

21. McKervey, M. A.; Rooney, J. J.; Samman, N. G. J. Catal. 1973, 30, 330.

22. Garin, F.; Gault, F. G. J. Amer. Chem. Soc. 1975, 97, 4466.

23. Dartiques, J. M.; Chambellan, A.; Gault, F. G. J. Amer. Chem. Soc. 1976, 98, 856.

24. Rooney, J. J. J. Catal. 1979, 58, 334.

25. Anderson, J. R. "Chemisorption and Reaction on Metallic Films", Academic Press: New York, 1971; Vol I and II.

26. Holland, L. "Vacuum Deposition of Thin Films", Chapman and Hall, Ltd.: London, 1966.

27. Mahaffy, P. M.; Hansen, R. S. J. Chem. Phys. 1979, 71, 1853.

28. Ertl, G.; Küppers, J. "Low Energy Electrons and Surface Chemistry", Verlag Chemie: Weinheim; 1974; Chapter 9.

29. May, J. W. Adv. Catal. 1972, 21, 151.

30. Ertl, G.; Kuppers, J. "Low Energy Electrons and Surface Chemistry", Verlag Chemie: Weinheim; 1974; Chapter 2.

31. Bhasin, M. M. In "Catalysis in Organic Syntheses 1976", Rylander, P.; Greenfield H., Eds.; Academic Press: New York, 1976; Chapter 2.

32. Christmann, K.; Ertl, G. Z. Natur. 1973, 28, 1144.

33. Chan, C. M.; Van Hove, M. A.; Weinberg, W. H.; Williams E. D. Solid State Commun. 1979, 30, 47.

34. Taylor, J. L.; Ibbotson, D. E.; Weinberg, W. H. Surf. Sci. 1978, 79, 349.

35. Davis, L. E.; McDonald, N. C.; Palmberg, P. W.; Keach, G. E.; Weber, R. E. "Handbook of Auger Electron Spectroscopy", 2nd ed.; Physical Electronics Industries: Eden Prairie, Minnesota, 1976.

36. Nieuwenhuys, B. E.; Somorjai, G. A. Surf. Sci. 1978, 72, 8.

37. Mimeault, V. J.; Hansen, R. S. J. Chem. Phys. 1966, 45, 224.

38. Dushman, S. "Scientific Foundations in Vacuum Technique", 2nd ed.; Lafferty, J. M., Ed.; John Wiley and Sons: New York, 1962.

39. Weast, R. C., Ed. "Handbook of Chemistry and Physics", 56th ed.; C.R.C. Press, Inc.: Cleveland, Ohio, 1975.

40. Masterson, P. B. Ph.D. Dissertation, Iowa State University, Ames, Iowa (1971).

41. Mikhail, R. H.; Brunauer, S. J. Colloid and Interface Science 1975, 52, 572.

42. Dalla Betta, R. A. J. Catal. 1974, 34, 57.

43. Roberts, R. W. J. Phys. Chem. 1963, 67, 2035.

44. Roberts, R. W. J. Phys. Chem. 1964, 68, 2718.

45. Martin, G. A. J. Catal. 1979, 60, 345.

46. Martin, G. A. J. Catal. 1979, 60, 452.

47. Martin, G. A.; Dalmon, J. A. C. R. Acad. Sci. Ser. C. 1978, 286, 127.

48. Nieuwenhuys, B. E.; Somarjai, G. A. J. Catal. 1977, 46, 259.

49. Nieuwenhuys, B. E.; Hagen, D. E.; Rovida, G.; Somarjai, G. A. Surf. Sci. 1976, 59, 155.

50. Blakely, D. W.; Somarjai, G. A. J. Catal. 1976, 42. 181.

51. Lehwald, S.; Ibach, H. Surf. Sci. 1979, 89, 425.

52. Arthur, J. R.; Hansen, R. S. J. Chem. Phys. 1962, 36, 2062.

53. Wright, P. G.; Ashmore, P. G.; Kemball, C. Trans. Faraday Soc. 1958, 54, 1692.

54. Ross, J. R. H.; Roberts, M. W.; Kemball, C. Trans. Faraday Soc. 1972, 68, 914.

55. Sárkány, A.; Tétényi, P. React. Kin. Catal. Lett. 1973, 9, 315.

56. Boudart, M. A. I. Chem. Eng. J. 1972, 18, 465.

57. Slaughter, M. D. Ph.D. Dissertation, Iowa State University, Ames, Iowa (1979).

58. Frennet, A. Catal. Rev. - Sci. Eng. 1974, 10, 37.

ACKNOWLEDGMENT

I would like to express my sincere gratitude to Dr. Hansen for his encouragement and support throughout my graduate career. I especially want to thank him for the freedom he gave me in conducting this research and the conclusions which have been reported herein. His comments and suggestions have always been appreciated.

I would like to express my thanks to the various support groups connected with the Ames Laboratory for the help they have given me throughout my stay here. The members of Dr. Hansen's research group, past and present, are thanked for the many productive discussions which we have had.

Finally I wish to thank my loving husband, Jack, without whose support I might not have completed this work. His many encouraging words will always be remembered.